Reviewed Preprint
v1 • February 3, 2026
Not revised

Reviewed Preprint
v2 • May 29, 2026
Revised by authors

Disentangling Cephalopod Chromatophores Motor Units with Computer Vision

Mathieu DM Renard[1,#], Johann Ukrow[1,#], Margot Elmaleh[1], Dominic A Evans[1], Yifan Wu[2], Xitong Liang[2,3,4,5], Gilles Laurent[1]

[1]Max Planck Institute for Brain Research, Frankfurt, Germany • [2]State Key Laboratory of Membrane Biology, School of Life Sciences, Peking University, Beijing, China • [3]IDG/McGovern Institute for Brain Research, Peking University, Beijing, China • [4]Peking-Tsinghua Center for Life Sciences, Academy for Advanced Interdisciplinary Studies, Peking University, Beijing, China • [5]Center for Quantitative Biology, Academy for Advanced Interdisciplinary Studies, Peking University, Beijing, China

For correspondence: g.laurent@brain.mpg.de

[#] Joint first authors

Competing interests: No competing interests declared

Funding: See page 28

Reviewing editor: John C Tuthill, University of Washington, United States

eLife Assessment

This **valuable** study uses a computer vision pipeline to infer the motor control of cephalopod skin, revealing that individual chromatophores exhibit anisotropic deformations and can be associated with multiple putative motor units. The evidence supporting these claims is **convincing**, and the authors present some limited electrophysiological validation of the findings from their computational analysis. This work will be of significant interest to biologists studying cephalopod behavior and motor control.

https://doi.org/10.7554/eLife.110074.2.sa4

Abstract

Cephalopod chromatophores are skin pigment organs that enable unmatched camouflage through rapid, flexible and neurally controlled deformation. Although their morphology is well known, the organization of their motor control is not entirely understood. Here, we combine high-resolution videography with a dedicated computer-vision pipeline (CHROMAS) to investigate chromatophore control and their likely innervation in *Euprymna berryi* and *Sepia officinalis*. By segmenting chromatophores into radial slices and analyzing anisotropic deformations, we applied dimensionality reduction (PCA) and source separation (ICA) to estimate the number and spatial influence of motor neurons responsible for the control of individual and groups of chromatophores. On average, four independent components were detected (suggesting innervation by four motor neurons), each forming contiguous petal-shaped domains rather than causing uniform expansion. Clustering thousands of components revealed motor units spanning multiple chromatophores, most involving fewer than 14 but occasionally spanning more widely. These motor units displayed a wide variety of geometries, ranging from compact local groups to elongated or fragmented structures; they often overlapped, with repeated co-innervation of chromatophore pairs occurring more often than expected by chance. Expansion was consistently faster and more stereotyped than relaxation, consistent with active contraction (corresponding to chromatophore expansion) and passive recoil (chromatophore contraction). Together, these results show that individual chromatophores are not singular or uniform pixels, but rather contrast elements that can be fractionated into smaller territories, themselves coordinated with those of other chromatophores. This geometry of neural control enables, among others, the generation of “virtual” chromatophores, i.e., functional groupings of adjacent chromatophore territories that act as single units, as well as that of noise in the distribution of pixel shapes.

Introduction

Coleoids, a subgroup of the cephalopod taxon which includes octopuses, squids, and cuttlefish, possess one of the most sophisticated camouflage systems found in nature. This extraordinary ability is mediated by arrays of pigment cells, known as chromatophores, which expand and contract to alter skin coloration and statistical patterning in response to motor command from the brain. The collective behavior of thousands or millions of chromatophores thus creates adaptive patterns that enable the animals to blend with their surroundings, evade detection by predators or prey and communicate with conspecifics (Hanlon & Messenger, 1988).

Cephalopod chromatophores differ from pigment cells in other animals: each chromatophore is a neuromuscular organ composed of a central pigment cell containing a cytoelastic sacculus, surrounded by 15–25 slender radial muscle fibers, themselves attached to an extracellular semi-stiff fiber mesh at their distal end (Messenger, 2001). The pigment granules residing in the elastic sacculus thus spread into a thin disc when the radial muscles contract due to motor neuron excitation, expanding the pigmented area. When the motor neuron input ceases, the chromatophore muscles relax, the elasticity of the sacculus causes it to recoil (and the cytoplasmic membrane to invaginate and fold onto itself), reducing visible coloration (or the size of this biological, expandable pixel). These muscle-driven, active expansion and elastic, passive retraction enable very rapid patterning and color changes, seen in no other biological coloration system. In addition to their unique neuromuscular structure, chromatophores occur in distinct color classes (typically yellow, red, brown, and black), each defined by the pigment (e.g, xanthommatin for yellow) and density of pigment granules they contain. These classes are linked to the age of the chromatophore (starting yellow and darkening over several weeks; Reiter et al., 2018), and usually migrate through the thickness of the skin, thus forming superimposed chromatic layers. Together they broaden the chromatic range available for patterning.

The basic neural circuit for camouflage patterning is well established: motor commands flow from visual processing centers (optic lobes) through basal lobes to the chromatophore lobes, where the somata of the motor neurons that directly innervate the muscles of the skin chromatophores reside (Boycott, 1961; Messenger, 2001). What remains unclear is how the axonal terminals of these motor neurons map onto individual and groups of chromatophores. Anatomical and physiological studies from Florey and colleagues (Cloney & Florey, 1968; Florey, 1969), as well as Dubas and Boyle (1985), provided evidence for polyneuronal innervation, with individual muscles or chromatophores under the control of several motor neurons. However, the number of inputs, their spatial organization, and the logic of motor unit formation remain unresolved.

This uncertainty limits our understanding of how the distributed neural activity that controls camouflage generates the details of body patterns. Treating chromatophores as uniform “pixels” ignores the possibility that subregions within each chromatophore could act as semi-independent effectors. Likewise, the degree to which chromatophores are coordinated in groups—forming motor units that span several chromatophores—has only been estimated qualitatively (Florey, 1969; Dubas & Boyle, 1985). These early anatomical and physiological studies suggested that individual motor neurons may innervate dozens to hundreds of chromatophores, but such estimates were indirect and limited in scope. More recently, computational approaches have begun to address this issue (Reiter et al., 2018), but these analyses considered chromatophores as indivisible units and provided only indirect evidence of motor-unit structure. No systematic, quantitative framework yet exists to describe the number, geometry, and overlap of chromatophore motor units on a large scale. We addressed this gap using high-resolution tracking of chromatophore dynamics combined with computational tools capable of disentangling overlapping motor inputs.

Results

Methodological development with Euprymna berryi

To establish a quantitative framework to analyze chromatophore motor control, we first focused on a model system with easily resolvable chromatophores. We chose the hummingbird bobtail squid, *E.*D*berryi*, because of large chromatophores, compact size, and rapid growth. We first show the analysis of a 30-s video dataset (1080 × 1080 px, 20 frames per second or fps) taken from a sedated hatchling (Fig. 1a; see Methods). Because our primary aim was to describe the composition and coordination of chromatophore motor units, it was important to examine animals in the absence of the descending commands that occur during active behavior. Spontaneous activity, typically mild and "noisy" was thus ideal to enable measurements of the motion correlations between chromatophores that reflected shared motor neuron drive, rather than shared correlations due to upstream motor neuron groupings by premotor circuits.

Chromatophores were segmented, each divided in polar (radial) slices and the areal variations of each slice across all successive time frames were measured, as developed and described in Ukrow, Renard et al., (2025). Chromatophore slices were then clustered using HDBSCAN (Hierarchical Density-Based Spatial Clustering of Applications with Noise, Campello et al., 2013), based on the temporal correlation of their size variations. This analysis revealed that clusters were composed of slices that lay both within and across individual chromatophores (Fig. 1b-c), with some chromatophores contributing to multiple clusters (Fig. 1d-f). Within a cluster, the orientation of each slice tended to align centripetally towards a virtual point located between the contributing chromatophores (Fig. 1g), effectively forming a closed "virtual chromatophore" rather than ring-like patterns. By "virtual chromatophore" we thus refer to a functional unit defined by the coordinated slice activities of adjacent chromatophores that share motoneuron innervation. Notably, smaller (yellow, less mature) chromatophores in the same region did not deform and therefore did not cluster, despite lying in the same apparent innervation fields. These inactive chromatophores proved to be very useful as stable anchors for motion tracking. If *E. berryi* allowed us to identify the important parameters of our analyses, this nocturnal species is only moderately interesting from a camouflage point of view. We thus transferred our methods to *Sepia officinalis*, a diurnal master of camouflage with large numbers and high density of chromatophores.

Analysis of chromatophore motion in Sepia officinalis

We applied CHROMAS to the skin of *S. officinalis*, where chromatophore density is roughly ten times higher and chromatophore dynamics are correspondingly harder to resolve. This animal (Fig. 2) was recorded under head fixation with and without sedation (HF+S and HF), conditions chosen to elicit spontaneous chromatophore activity required for correlation analysis (see above), using 8K video recordings and visible implant elastomer (VIE) markers for consistent region identification across days or weeks (see Methods). We focused on a small region at the center of the dorsal mantle (Fig. S1) and analyzed sections (0.5 by 0.5 mm) of a 108-s HF video segment (2160 images) and a 20-s HF+S segment (400 images), that together yielded 3,285 segmented individual chromatophores. These datasets provide the basis for the following quantification of chromatophore anisotropic expansion and motor unit identification.

Interpretation of fine single-chromatophore motion

We performed PCA on the 36Lslice time series of each chromatophore (see Fig. 2a for a single chromatophore) and from it estimated the number of principal components (PCs) needed to explain most of the variance in the motion data. The number of relevant components was determined by identifying the point of maximum curvature in the cumulative explained variance curve, as implemented in the CHROMAS pipeline (Ukrow, Renard et al., 2025; see Methods). In Fig. 2b, this point corresponds to PC5 (red dashed line), beyond which additional components contribute negligibly to the explained variance. Over 1,829 chromatophores in the HF + S dataset, this approach yielded 3.715 ± 1.211 PCs per chromatophore on average (Fig. 2c). To test for an

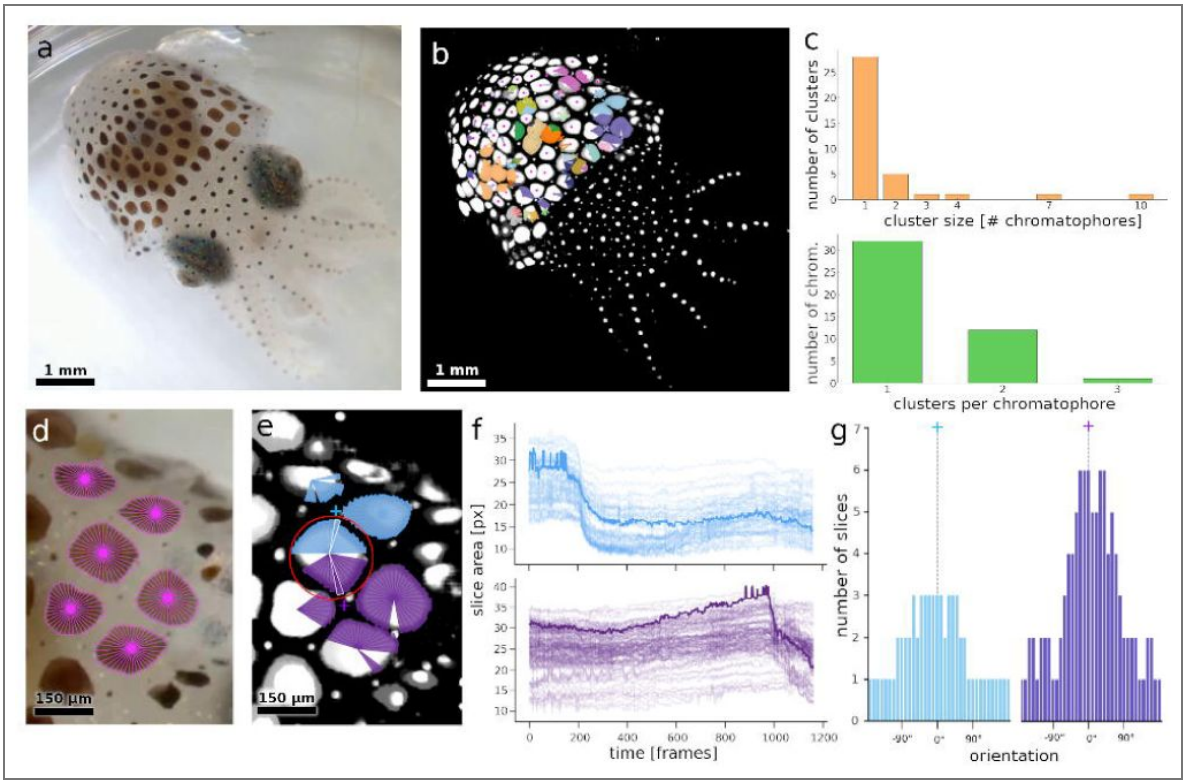

Figure 1. Identification and characterization of putative chromatophore motor units in *E. berryi*.

a) Example HD-video frame extracted from a *E. berryi* recording. b) Visual representation of presumed motor units. Colors represent motion clusters of chromatophore slices grouped together by covariation using the HDBSCAN algorithm. Segmented chromatophores shown in white, with epicenters marked as magenta dots. Coloured clusters indicate presumed motor units based on slice motion correlation. Outlier slices are omitted for clarity. c) Number of chromatophores per cluster size, and frequency of chromatophores belonging to multiple clusters. d) Zoom on the frame shown in a, with detected slices overlaid in magenta. e) Zoom on two overlapping motor units from b. The central chromatophore (red circle) contributes slices to both the blue and the purple clusters. Cluster centers of mass, calculated from the epicenters of the chromatophores belonging to each cluster, are shown as colored crosses. This illustrates two “virtual chromatophores”, where coordinated activity spans slices from several chromatophores. f) Surface areas of slices belonging to each cluster over time. In bold, the surface areas of the slices highlighted in white in e. g) Distribution of slice orientations relative to the motor unit’s center of mass.

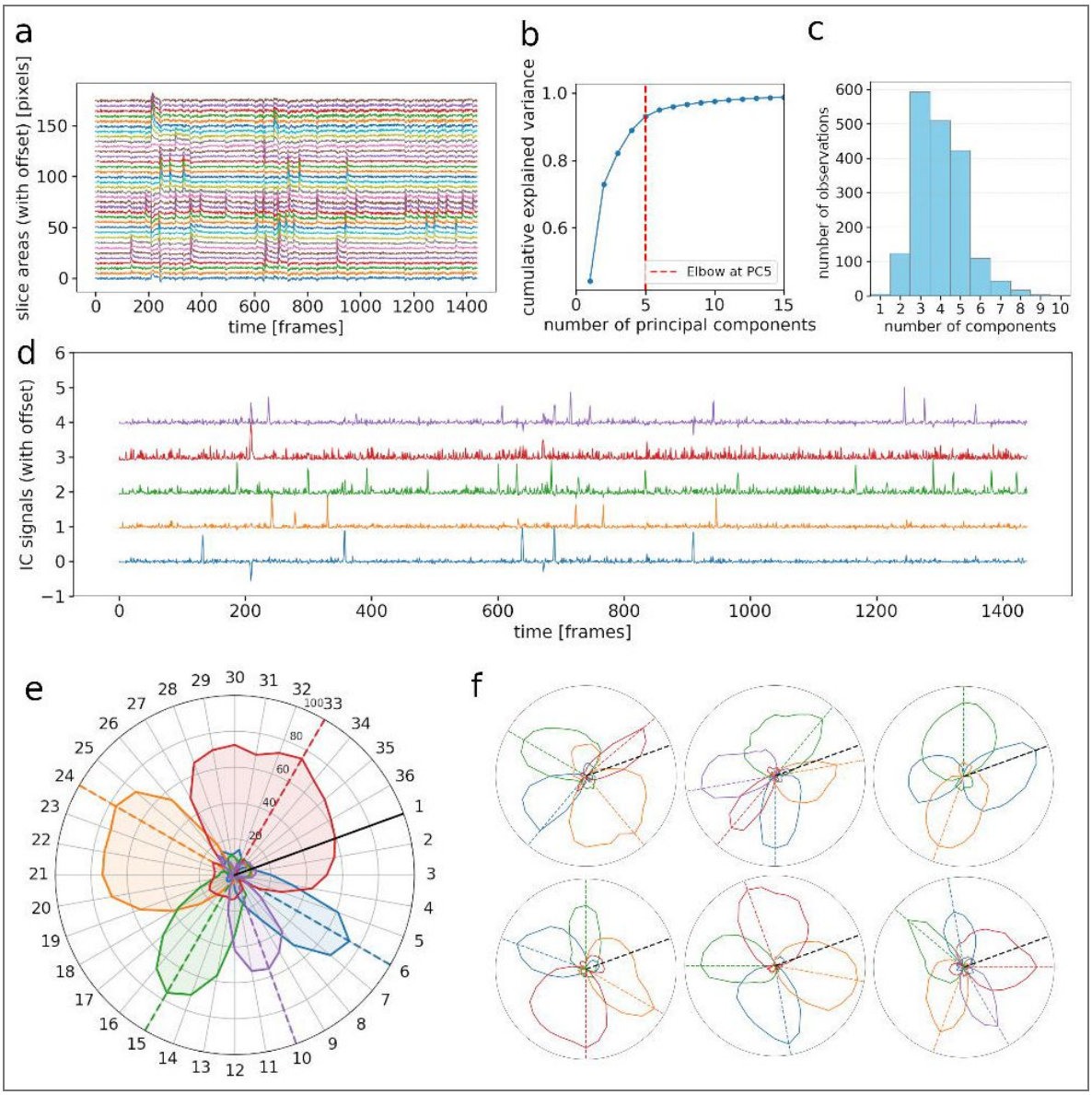

Figure 2. Multiple innervation of individual chromatophores.

a) Activity traces (surface area as functions of time) of 36 polar slices from a single chromatophore, offset vertically pairwise by 5 pixels for clarity. Each trace represents the positive, detrended change in surface area over time, highlighting expansion dynamics while excluding negative (contraction) phases (see Methods), assumed to be passive. b) Cumulative explained variance plot for Principal Component Analysis. Relationship between number of principal components and explained variance, with PCs ranked by decreasing contribution. Red dashed line corresponding to greatest slope change (here PC5) (see Methods). c) Histogram showing the number of principal components identified per chromatophore across the dataset. d) Independent sources acting on the 36 slices of a single chromatophore, extracted with Independent Component Analysis. In this case, the chromatophore is controlled by 5 independent sources that likely correspond to 5 distinct motor neurons. e) Polar plot representing the influence of each source (motor neuron activity) on each slice. Black line indicates the first radial slice; influence of a source on a slice expressed in % (radial scale). f) Examples of PCA-ICA analyses run on six other chromatophores.

effect of sedation, we repeated the analysis on 1,456 chromatophores in the head-fixed, not sedated condition (HF), and obtained 3.683 ± 1.224 PCs. A Welch's t-test reveals no significant difference between these two conditions (t = 0.21, p = 0.83; Cohen's d = –0.03).

The number of dominant explanatory components identified by PCA was then used to initialise an Independent Component Analysis (ICA). This operation extracted the dynamics of the putative underlying sources (Fig. 2d) and revealed their spatial influence on individual chromatophore slices (Fig. 2e–f). Each independent component—which we interpret as the signature of firing activity in a single motor neuron—was overlaid onto the 36 equal polar slices to generate a detailed influence map for each chromatophore (Fig. 2e-f). Across our dataset, the putative motor neurons, so identified, innervated between three and sixteen slices per chromatophore. Importantly, these targeted slices consistently formed contiguous domains around the chromatophore's circumference. The influence profiles frequently adopted a petal-like shape, characterised by a peak in one polar position and a gradual tapering of influence across the adjacent slices. This parcelated representation suggests the topography of motor innervation of single chromatophores, and provides the most likely explanation for the observed anisotropic expansion patterns of single chromatophores.

Structure and size of chromatophore motor units

Affinity-propagation clustering of the 6,795 independent components (ICs) extracted from 1,829 chromatophores (HF+S dataset) yielded 754 clusters, and thus putative motor units (MUs). Each putative MU comprised a mean of 9.003 ± 4.755 ICs, and 95.877 ± 7.566 % of these MUs spanned multiple chromatophores, indicating extensive multi-chromatophore innervation (Fig. 3a-b). For this spatially bounded dataset (Fig. 3b), the cluster-size distribution was skewed, with 90 % of motor units innervating fewer than 14 chromatophores (Fig. 3c). We analyzed the same chromatophores under our two conditions: HF and HF+S. A Welch's t-test revealed no significant difference in the number of components per MU between the two groups (HF = 8.551 ± 5.753, n = 626, vs. HF+S = 9.003 ± 4.755, n = 754; t ≈ –1.57, p = 0.12).

The spatial relationship between chromatophores belonging to the same putative MU was assessed by calculating pairwise distances and convex hull areas of putative MU clusters. The global nearest-neighbor distance (NND)—defined as the average shortest distance from each chromatophore to its closest neighbor across the entire dataset—was 6.130L±L1.589Lμm. In contrast, the mean within-cluster NND was 40.548 ± 46.946Lμm, indicating that chromatophores grouped within the same motor unit are not limited to immediate neighboring chromatophores. The corresponding furthest distance—defined as the greatest distance between any two chromatophores within a cluster—was 228.96 ± 94.36 μm. The corresponding global value (361.50 ± 49.80Lμm) depends directly on the field of view of the camera and is thus less informative.

To quantify spatial coverage, the convex hull area was measured for each cluster. (The convex hull area refers to the area of the smallest convex polygon that fully encloses a given set of points.) The distribution of these areas (Fig. 3d) shows that most clusters occupy relatively small regions. Across 754 clusters, convex hull areas ranged from 25.18 μm^2 to 915,087.66 μm^2, with a median of 136,199.10 μm^2 and a mean of 209,793.70 μm^2. Ninety percent of clusters had a convex hull area smaller than 51,513.25 μm^2 (or 0.0515 mm^2, the equivalent of a fine grain of sand). Figure 3e-f illustrates the relationships between spatial and compositional features of motor units. A positive correlation (r =L0.66) was observed between cluster area and chromatophore count (Fig. 3e), while a weak negative correlation was found between area and chromatophore density (r = –0.14) (Fig. 3f), and between chromatophore count and density (r = –0.14). These relationships suggest that clusters occupying larger areas tend to have more chromatophores (Fig. 3e), but at lower density (Fig. 3f).

We next examined the secondLorder coLoccurrence, defined as the number of unique chromatophore pairs that were parts of at least two distinct motor units. This number was 1,073 in our dataset and was compared to the value expected under a null hypothesis of random paired assignments. A set of 1,000 random permutations yielded a distribution shown in Fig. 3g, and an expected mean value of 263.72 ± 16.94 pairings. The highly significant difference between these

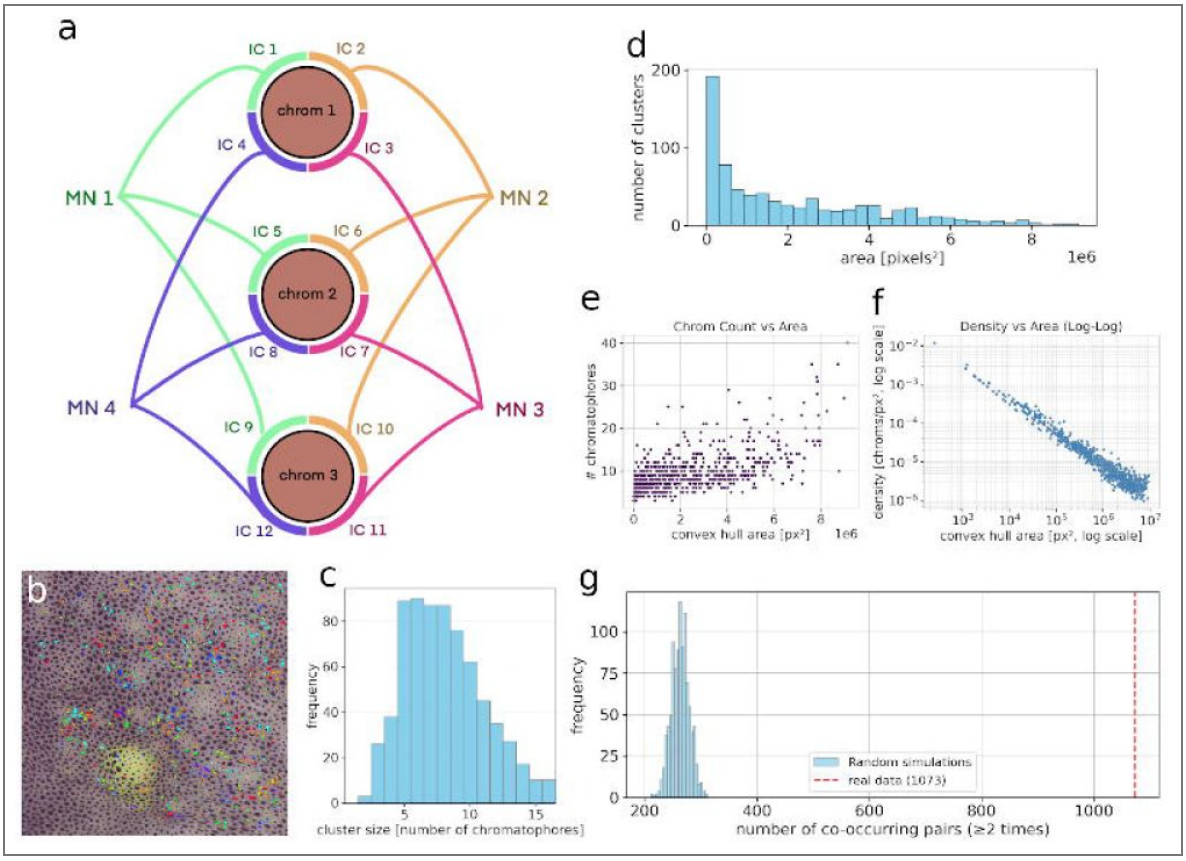

Figure 3. Identification of putative motor units.

a) Schematic representation of derived chromatophore innervation by motor neurons. Each chromatophore is depicted as a circle, with arcs around them representing independent components identified by ICA, each interpreted as corresponding to the zone of influence of a single motor neuron on that particular chromatophore. One goal of this clustering was to reveal shared chromatophore innervation and thus, motor units. Colors and lines connecting IC arcs indicate that they belong to the same motor unit, highlighting the shared innervation pattern across multiple chromatophores. b) A small number of clusters of size 3 to 5 are mapped back on the original image for visualisation. c) Distribution of cluster size (size in number of IC). For visualisation, the graph was truncated to show over 90% of the data. d) Distribution of cluster convex hull areas, showing a right-skewed profile with most clusters occupying smaller areas. All values are reported in pixel^2 (px^2); note that the main text reports corresponding measurements in µm^2 after conversion (10 pixels = 1 µm, thus 1 px^2 = 0.01 µm^2). e) Relationship between chromatophore count and convex hull area for each cluster. f) Chromatophore density (chromatophores per pixel^2) as a function of convex hull area, plotted on a log-log scale. The inverse relationship reflects decreasing density in larger clusters. g) Histogram showing the distribution of second-order co-occurrence counts—defined as the number of chromatophore pairs co-occurring in at least two clusters—across 1000 randomised datasets (blue). Randomisations preserved both the number of clusters and the number of memberships per chromatophore. The red dashed line indicates the observed experimental value, significantly higher than expected by chance.

two values (Z = 49.36, p < 0.0001) indicates that co-innervations are not random, and suggests the existence of cooperative or joint-causality mechanisms for the innervation and control of nearby chromatophores.

The spatial structure of putative motor units displayed a wide range of configurations (Fig. 4). Some clusters were compact, with chromatophores arranged closely together and spanning small distances (e.g., panels a–d). In many cases, clusters (i.e., MUs) shared chromatophores, resulting in overlapping network structures (e.g., panels e–f). Other clusters exhibited more elongated or linear profiles (e.g., panel g), with chromatophores extending over a longer axis. In addition, mixed profiles were observed, where a core group of closely spaced chromatophores was connected to one or several distant chromatophore(s) (e.g., panels g and h). Because our field of view did not encompass the mantle in its entirety, our analysis will have missed large motor units spread over very large areas, if they exist.

Dynamics of chromatophore expansion and contraction

Because chromatophore deformations are caused by active expansion (radial muscle contraction) and passive (elastic) recovery (radial muscle relaxation), the two phases of chromatophore deformation have different dynamics (fast expansion, slower recovery). We tested whether these kinetic differences could be detected in our videographic measurements at 20 fps, i.e., at sampling rates low compared with those of electrophysiology (Florey, 1969). We analyzed expansion and recovery processes on individual slices, so as to isolate the activity of different presumed radial-muscle groups within each chromatophore. We focused on chromatophores with high activity levels to ensure clear detection of expansion and contraction phases and accurate estimation of their respective speeds and durations.

Although very variable, our data showed that chromatophore expansion is significantly faster and more stereotyped than contraction across chromatophores (Fig. 5 and S2). By separating events by amplitude, our videographic approach captured expansion–contraction dynamics across a wide range of events. These results indicate that these kinetic features can be detected with the temporal resolution of our video-imaging. Specifically, across a subset of 10 active chromatophores (from the HF+S dataset), expansion phases occurred at an average speed of 0.667 ± 0.590 pixels/frame, compared with 0.422 ± 0.557 pixels/frame for the contraction (n=2157 events). This difference was significant (paired t-test, t = 19.50, p < 0.001). In our datasets, 10 aligned pixels span 1 µm. Expansion events were spread on average over 4.41 ± 1.91 frames vs. contractions, 5.90 ± 3.50 frames. These results are thus consistent with the basic mechanisms of chromatophore motor activation, and highlight our technique as a reliable tool to study certain aspects of radial muscle biomechanics.

Direct activation of single chromatophore motor neurons (Euprymna berryi)

The above observations in *Sepia* were based on high-resolution video image data of spontaneous resting activity, enabling the simultaneous monitoring of large regions of skin and thus, the simultaneous tracking of large numbers of chromatophores and measurements of their motion correlations. To test for the validity of the approach, we also carried out combined video imaging and whole-cell patch-clamp recordings of single motor neurons, thus enabling the direct control of single-motor neuron discharge. Our goal was to test, on a small scale, the validity of the large-scale motion-correlations approach based on measurements of spontaneous activity. In particular, we wished to check directly whether individual chromatophores are anisotropically controlled by multiple motor neurons with polarised action (as suggested by the deformation “petals” in Fig. 2), and whether the action of individual motor neurons on a field of nearby chromatophores is usually directional, with expansion vectors oriented towards a virtual center of mass.

To this end, we returned to *Euprymna* (to increase the probability of finding both motor neurons and corresponding chromatophores, because the number of chromatophores in this species is small), patched a motor neuron in the posterior chromatophore lobe and looked for the patch of

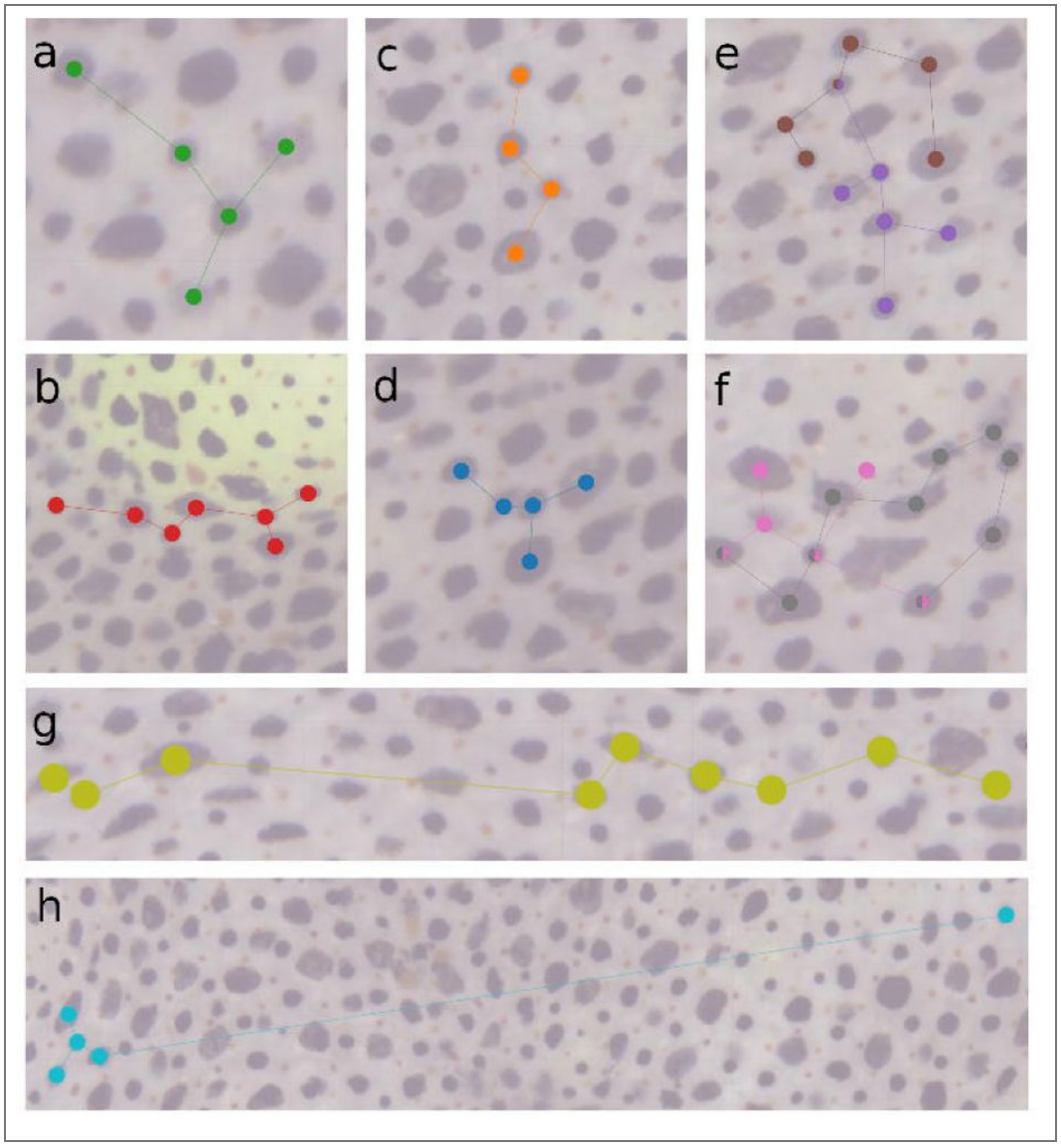

Figure 4. Spatial organization of putative motor units.

Chromatophores belonging to the same correlated-motion cluster, or putative MU, are shown as colored dots connected by lines. a-d) Compact clusters. e-f) Overlapping clusters with shared chromatophores. g) Elongated cluster with a linear structure. h) Mixed profile featuring a core group of adjacent chromatophores connected to a single, distant chromatophore.

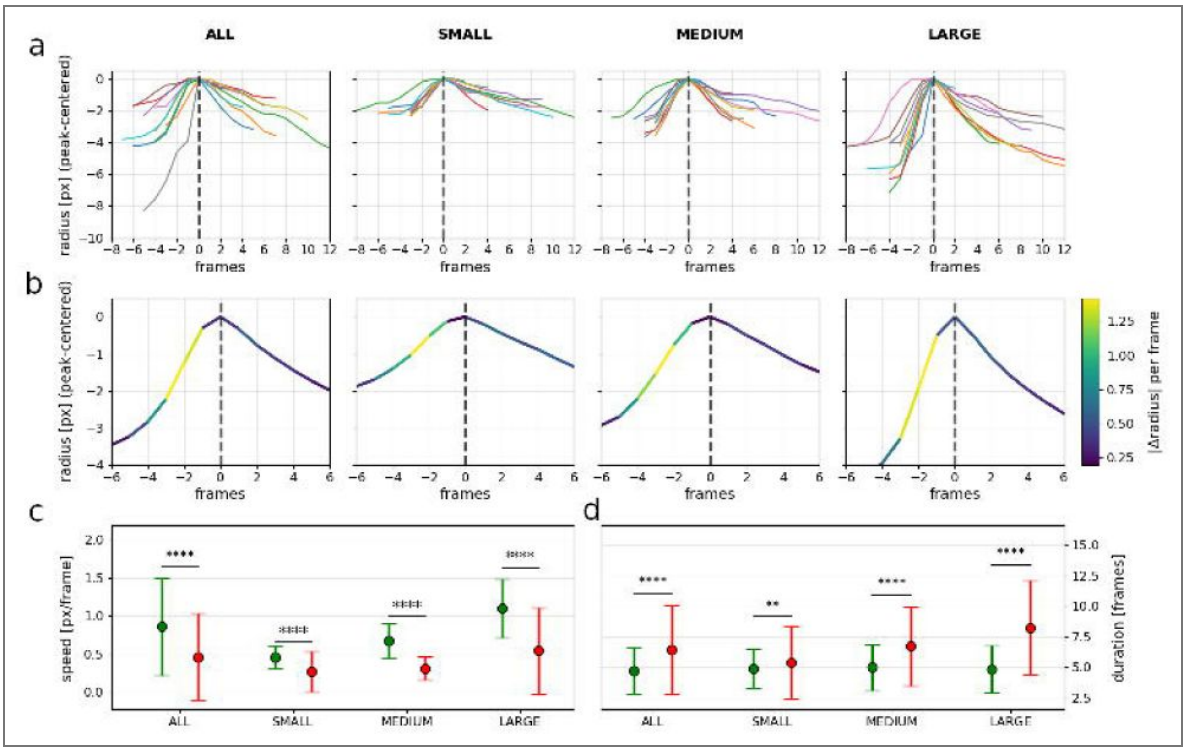

Figure 5. Composite summary of chromatophore slices expansion–contraction dynamics.

Events are first filtered to remove very small peaks (expansion amplitude ≤ 15% of the observed amplitude range). Remaining events are split by expansion amplitude percentiles: SMALL = lower tail, MEDIUM = central band, LARGE = upper tail. Within each tail band, outliers in either amplitude or speed are removed using Tukey's IQR rule, and statistics are computed on the remaining events (see Methods). a) Peak-aligned event segments (10 randomly selected events per column) for each group. Traces are shifted to align at the peak (t=0). Same *y* calibration in the four panels. b) Mean event profile for each size group, where each segment is color-coded by instantaneous size change (|Δradius| for pairs of consecutive frames); LUT at right. Same *y* calibration in the four panels c) Means ± SDs of chromatophore size change (px/frame) for expansion (green) and contraction (red) phases. Statistical significance evaluated using paired t-tests between expansion and contraction phases (n = 2157 event pairs). Asterisks indicate significant paired differences $p < 0.05$ (*), $p < 0.01$ (**), $p < 0.001$ (***), and $p < 0.0001$ (****). d) Same as in c but for event duration (in frames).

skin containing the innervated chromatophores. Once those had been identified, we injected a 1s-long direct current in the patched motor neuron to cause sustained firing (Fig. 6a), and observed the effect of this activation on the chromatophores (Fig. 6b and Supplementary movie 1). Here the motor neuron innervates five nearby chromatophores, causing a partial, directed, petal-like expansion of each one towards a virtual common center located near their common center of mass. Detecting this innervation pattern in this example proved difficult using spontaneous activity alone (*i.e.*, excluding the electrophysiological recording), due to the small amplitude of the chromatophore deformations caused by single motor neuron action potentials. These observations were repeated in 16 motor neurons from 12 different animals, revealing a detectable effect in 4.38 ± 0.55 chromatophores (mean ± SEM, n = 16) (Fig. 6c; videos provided in the Data Availability section). Note however that the expansion of chromatophores by single-motor neuron electrical activation was not always anisotropic (Fig. 6c - bottom right), suggesting that some chromatophores in *Euprymna* are controlled by single motor neurons (or that motor neurons with a common chromatophore target may be electrically coupled). We conclude that our quantitative videographic approach based on the analysis of spontaneous chromatophore deformations in *Sepia* reveals features that are consistent, but on a large scale, with those revealed by focal motor stimulation.

Discussion

Our results extend early focal electrophysiological observations to large physical scales, thanks to the quantitative and easy-to-use videographic methods that we developed recently (Ukrow, Renard et al., 2025). Messenger (2001), drawing on Florey's electrophysiological studies (Florey, 1969), suggested that chromatophores are controlled by at least four motor neurons. Our decomposition consistently revealed three to four independent causes for individual chromatophore deformation. Our results match and support these early inferences, but are here based on direct analysis of thousands of chromatophores in parallel. Likewise, Dubas (1985, 1986) estimated that a single motor neuron may innervate tens to hundreds of chromatophores, typically of the same color. Our clustering revealed units of variable size, typically around ten chromatophores in *S. officinalis* but sometimes extending much further (up to thirty), matching her conclusion that motor fields are both distributed and overlapping. We never detected, however, motor units containing many tens to hundreds of chromatophores with our technique. This may be due to the generally small expansions caused by spontaneous motor neuron discharge, presumably usually limited to single action potentials; it is possible also that the gain of motor neuron-chromatophore transfer varies over the spatial extent of an innervation field. If so, only some of the targets of a motor neuron would be identifiable with our methods.

Contrary to mature skeletal muscle innervation in vertebrates (Henneman, 1957; Kernell, 2006), individual invertebrate muscle fibers often receive convergent excitatory inputs from more than one motor neuron (Hoyle, 1955; Bullock & Horridge, 1965; Sasaki & Burrows, 1998, Florey, 1969; Dubas & Boyle, 1985). The nature of our videographic methods was not sufficient to resolve chromatophore fiber poly-innervation, if it exists. If anything, however, the adjacent deformation "petals" we identified rather suggest adjacent, but non overlapping territories of muscle-fiber innervation by individual excitatory motor neurons. The patterns of correlated deformation of multiple chromatophores were consistent with earlier findings (Dubas & Boyle, 1985; Reiter et al., 2018) that individual motor neurons innervate chromatophores of the same colour. Given the systematic intercalation of yellow and brown chromatophores in the skin (in which chromatophore color is correlated with chromatophore age; Reiter et al., 2018), the monochromatic innervation patterns, combined with their great spatial precision, indicate a remarkable degree of local control of chromatophore innervation by motor neurons in *Sepia*.

Most strikingly, our results reveal a phase offset between the anatomical matrix of chromatophores and their functional innervation. Each chromatophore can be subdivided into several (typically three to four) independently controlled zones, each containing an adjacent subset of the 15–25 radial muscles that control each chromatophore; these zones typically cut across neighboring chromatophores. This results in the possible generation of "virtual

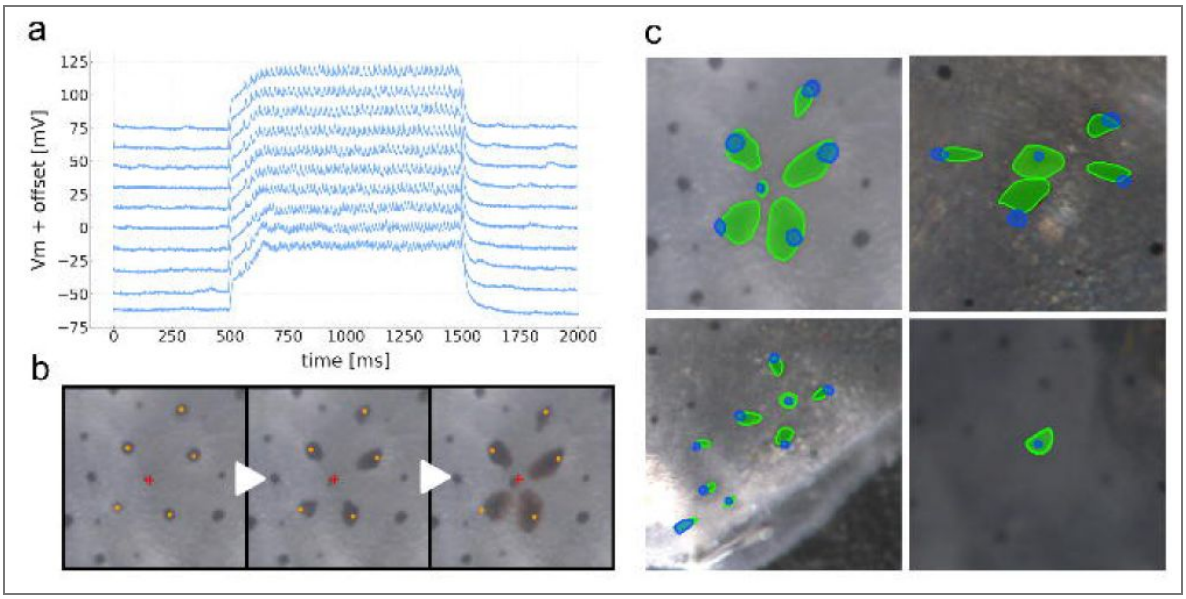

Figure 6. Patch clamp stimulation of chromatophore-lobe motor neuron.

a) "Patch-clamp recordings from a chromatophore-lobe motor neuron. Ten consecutive sweeps are shown, vertically offset for clarity and downsampled x4 (from 100 to 25 kHz). b) Sequence of video stills showing chromatophore expansion elicited by stimulation of the same motor neuron as in a. In orange, chromatophore epicenters, defined as the center of mass at the frame where the chromatophore is in its most contracted state. Each chromatophore expands anisotropically toward a common center of innervation (approximated as a red cross). c) Composite images showing chromatophore outlines before (blue) and during stimulation (green). The first three examples display anisotropic expansion across several chromatophores within a single motor unit—the first example is the same motor unit shown in a–b. The last example shows isotropic expansion of a motor unit composed of a single chromatophore.

chromatophores", or chromatic zones formed by the convergence of the quadrants of nearby chromatophores. This suggests that the smallest addressable units of cephalopod skin are not necessarily single chromatophores but rather topographically ordered subsets of radial muscles, spread over multiple chromatophores and grouped by their shared motor neuron. This view modifies and extends Packard's (1982) billboard analogy: chromatophores are not isolated "billboard lightbulbs" but overlapping zones wired through multiple control lines. Such an arrangement implies strong developmental constraints on wiring while simultaneously enhancing the flexibility of body-pattern generation.

Our analyses suggest that chromatophore control operates through overlapping innervation fields that often do not coincide with the anatomical boundaries of individual chromatophores. In *E. berryi*, motor units tended to be compact and converged toward points between neighboring chromatophores, effectively creating "virtual chromatophores" composed of partial contributions from adjacent cells. Several mechanisms could underlie this organization. Developmentally, axons may innervate radial muscles opportunistically within restricted skin regions rather than selectively targeting individual chromatophores, leading to fields that span across cells. The inactivity of younger orange chromatophores embedded within active fields and the independent control of yellow chromatophores suggest that innervation may also be stratified by depth, consistent with the layered organization of chromatophore colors (Messenger, 2001) and the developmental processes shaping this system (Packard, 1982). As chromatophores age and change color, vertical migration within the skin might bring them within other motor innervation territories and lead to their reinnervation. Our techniques will now enable the study of the development of chromatophore innervation and possibly, of their reinnervation as they age and change pigment.

Our videographic approach also provides sufficient temporal resolution to resolve some aspects of radial-muscle kinetics, opening avenues to study chromatophore biomechanics and, ultimately, to separate the contributions of intertwined forces, including but not limited to radial muscles, elastic pigment sacs, and intercellular coupling, to expansion dynamics.

Functional implications

Although motor units are often composed of multiple chromatophore sectors rather than whole chromatophores, the resulting pigment fields can be visually indistinguishable from those produced by full-chromatophore control. This fragmented organization could simply reflect wiring constraints, but it may also confer functional advantages. By recruiting sectors from different chromatophores, motor units introduce irregular contours, asymmetries, and non-uniform shapes, expanding the expressive range of the skin and reducing geometric repetitiveness in pattern textures. Sector-based units may therefore permit finer spatial modulation or realistic pattern "noise", particularly during partial activation states.

Most motor units we observed fell below 51,513 μm^2 in convex-hull area, roughly equivalent to a ~227 µm square. This scale matches the grain size of very fine sand (125–250 µm; Wentworth, 1922; Blott & Pye, 2012), which dominates Mediterranean coastal habitats where *S. officinalis* is common (Sandulli et al., 2010; Bettoso et al., 2016; Dauvin et al., 2017; Asensio-Montesinos et al., 2022). Such correspondence suggests that motor-unit resolution may be ecologically tuned to substrate textures, providing effective camouflage without incurring the energetic costs of finer-grained control.

Shared innervation of chromatophore sectors by multiple motor neurons may enable gradual, fluid transitions between patterns. As one unit ramps down and another ramps up, overlapping territories smoothen otherwise abrupt boundaries. These overlaps could also underlie dynamic displays such as the "passing cloud" (How et al., 2017; Laan et al., 2014; Mather & Mather, 2003), in which waves of activity propagate seamlessly across the skin.

Motor units exhibited diverse geometries, from compact clusters to elongated or fragmented ensembles. Such variability may be functionally specialized: tight units supporting sharp edges or high-contrast motifs, while dispersed units contribute to gradients or subtle textures. This

architecture resembles receptive-field mosaics in sensory systems. Just as retinal ganglion cells (Masland, 2012) or cutaneous mechanoreceptors (Mountcastle, 2005) vary in size and density to capture distinct features, chromatophore motor units form an outward-facing mosaic of overlapping "projective fields" that compose complex visual patterns.

Technical issues

Our non-invasive recordings and large-scale analyses rely on indirect inference based on spontaneous correlated motion rather than direct electrophysiological measurements. The great advantage of this approach is that it enables large-scale measurements in freely behaving animals. This would be impossible with electrophysiological recordings. Chromatophore expansion served as a proxy for radial muscle contraction, itself a result of motor neuron activity. One limitation is that the inferences we make about motor neuron activation are indirect. Using simultaneous motor neuron recordings and chromatophore imaging in reduced preparations of the brain and mantle skin, we could nevertheless confirm several of our interpretations using direct motor neuron activation. The non-isotropic action of individual motor neurons on individual chromatophores and the converging expansion of nearby chromatophores under the action of a shared motor neuron, for example, could each be confirmed directly. We observed, however, that the direct-current injections needed to generate a detectable chromatophore expansion were often prolonged, causing the production of trains of action potentials in the patched neuron. Spontaneous chromatophore expansion, however, is probably caused by spontaneous and isolated (i.e., single) motor neuron action potentials. It is possible, therefore, that what can be detected using our image analysis approach on spontaneous activity underestimates the true patterns of innervation. This will be especially true if the gains of the many neuromuscular junctions made by a single motor neuron vary across its output field. Only the stronger outputs will lead to detectable motion. (Note that the petal shape of the chromatophore expansion quadrants suggests a gradient of innervation strength—central peak flanked by decreasing motion amplitude over each corresponding quadrant.) We also observe that, to be interpretable, the patterns of chromatophore expansion during spontaneous "noisy" activity should be as decorrelated as possible. If for example, two motor neurons share a presynaptic excitatory drive, they may often fire together when their common presynaptic neuron is active, leading to the erroneous delineation of motor units. Our approach must therefore be applied in conditions of minimal activity, ideally during the apparent spontaneous flicker that is usually observed in resting animals.

Chromatophore slice dynamics were estimated from membrane deformation rather than direct detection of muscle insertion points; similarly, putative motor units were defined by clustering of correlated activity profiles. While such proxy-based approaches involve multiple inferential steps, they are routinely used in neuroscience and physiology to extract functional information from imaging data—for example, inferring spiking from calcium fluorescence or estimating muscle activation from high-speed video recordings. Our strategy applies the same principle to chromatophore dynamics, providing scalable, non-invasive access to living animals.

The two principal clustering strategies which we settled on and used—HDBSCAN, with *E. berryi* during pipeline development, and Affinity Propagation, adopted as a refinement for *S. officinalis*—make different assumptions about cluster structure. In particular, Affinity Propagation groups sectors based on pairwise similarity of activity dynamics rather than local density in feature space. Although both approaches yielded consistent biological insights, it should be noted that inferred motor units are not insensitive to algorithmic choices and should be interpreted with this in mind. More generally, clustering constitutes a form of model selection, and alternative algorithms may reveal complementary aspects of motor-unit organization.

Just as in any imaging approach, spatial and temporal sampling considerations represent important constraints. In *S. officinalis*, recordings were restricted to small regions of the dorsal mantle, precluding whole-body comparisons and leaving open whether motor-unit organization is conserved across skin regions. Developmental factors further narrowed the available time windows for observation: chromatophore overlap in growing *E. berryi* hatchlings and low spontaneous activity in young *S. officinalis* juveniles restricted the stages suitable for analysis. In

this context, the large, spatially dispersed motor units observed in *S. officinalis* may not represent a universal architecture; they could reflect the developmental stage of the individuals we studied or species-specific ecological requirements. Previous reports based on more limited, but electrophysiological stimulation experiments, suggest considerable diversity across cephalopods, with Dubas (1985) describing widely distributed motor units in octopus and Florey (1969) reporting more compact units in squid. The extent to which motor unit size and shape vary as functions of species, position on the body, and developmental stage, will need to be examined.

The complex mechanics and innervation patterns of chromatophores introduce ambiguities. Elastic recoil of the pigment sac and mechanical coupling between adjacent radial muscles likely propagate forces beyond the site of neural activation, producing secondary deformations (of unknown amplitude) in neighboring slices. In addition, overlapping motor neuron axons could converge onto the same set of radial muscles, in which case a single slice would at times reflect the combined drive of multiple neurons. Together, these factors make it difficult to determine where the influence of one motor neuron ends and that of another begins. As a result, our estimates should be viewed as functional partitions of activity rather than definitive anatomical boundaries.

In conclusion, we developed an image analysis pipeline (Ukrow, Renard et al., 2025) and used it to analyze the structure of chromatophore expansion and shape control in two species of coleoid cephalopods, from high resolution movies of freely moving animals. This approach revealed many fine features at the distal end of this highly specialized motor system. By identifying first the motor units, as done here, it may become possible to reveal important aspects of their presynaptic drive and thus make precise and testable predictions about the organization of this remarkable neural system.

Methods

Chromatophore video acquisition and analysis

Animals

All research and animal care procedures related to video acquisition of chromatophores and analysis were carried out in Frankfurt, in accordance with the institutional guidelines that are in compliance with national and international laws and policies (DIRECTIVE 2010/63/EU; German animal welfare act; FELASA guidelines). The study was approved by the appropriate animal welfare authority (Regierungspräsidium Darmstadt) under approval number V54-19c20/15-F126/2012.

Hummingbird bobtail squids *Euprymna berryi* and European cuttlefish *Sepia officinalis* were hatched from eggs laid in house and reared in a seawater system. The closed system contained artificial seawater (ASW; Instant Ocean) with a salinity of 33-36 ppt and pH of 8.1-8.4. Water quality was monitored continuously and was tested regularly. The housing temperature was different in function of the species. Aqua Medic *Tri Complex* supplied macro- and trace elements continuously. A constant water through-flow resulted in 5 complete water exchanges per hour. Room illumination provided a 12 h–12 h light–dark light cycle with gradual on- and off-sets at 07:00 and 19:00. Enrichment consisted of natural fine-grained sand substrate, artificial plastic plants and translucent red plastic houses. Both species were fed live food (either *Neomysis* spp. or small *Palaemonetes* spp.) twice per day.

E. berryi were reared in a seawater system at 20-26 °C. The filtration systems included filter bags, protein skimmer, biofilter, UVC-sterilisator and heater. The adult animal groups were housed in 300-L plastic tanks, juveniles in plastic boxes of 18-36 L. Experimental animals of unknown sex, just a few days after hatching, ranging from 3 to 6 mm in mantle length, were selected for healthy appearance and calm behavior.

S. officinalis were reared at 18-20 °C. The filtration systems included drum filter, protein skimmer, biofilter, UVC-sterilisator and chiller. The animals were housed individually in 30-90 L PVC tanks with a constant water through-flow resulting in 5 complete water exchanges per hour. Animals

above 50 mm in ML were fed once per day defrosted fish or shrimp. Experimental animals of unknown sex, 5 days to 10 months after hatching, ranging from 5 to 100 mm in mantle length, were selected for healthy appearance and calm behavior.

Arena and filming equipment

E. berryi: the arena design aimed to confine the hatchlings within an area fully covered by the camera's field of view. The resulting arena measured 10 cm × 10 cm × 3 cm in height and included a conical sub-arena with a direct water inflow (Fig. S3a). This cone featured small holes allowing water to outflow into a larger surrounding chamber. The design incorporated a glass lid to reduce visual distortion by enabling direct water-glass contact and improving image clarity. Additionally, the arena floor included a glass surface to permit imaging from below. A peripheral "trench" area surrounding the chamber directed excess water through outflow tubing, ensuring continuous circulation. For recording, we used a Basler Ace 2 (a2A2590-60ucPRO, Basler, Ahrensburg, Germany) equipped with a Kowa lens (LM25JC10M, Kowa, Nagoya, Japan). The imaging configuration enabled 1920 × 1920 px recordings corresponding to a 1 × 1 cm field of view, large enough to encompass the whole body of *E. berryi*. Illumination was provided by a custom-built LED ring mounted above the imaging arena and controlled through a custom software to modulate light intensity cyclically during recordings. Recordings were performed inside a custom sound- and light-proof enclosure lined with acoustic foam to dampen external vibrations and reflections. The box contained the imaging arena, camera, and LED ring, ensuring stable sensory conditions during recordings.

S. officinalis: the arena measured 20 cm x 30 cm x 10 cm, was made of acrylic glass material and featured a height-adjustable cover along with designated water entry and drainage points. Four LED lamps were mounted on adjustable side brackets around the arena, allowing control over their height, position, and angle (Fig. S3b). For recording we used the Basler CoaXPress 2.0 boA9344-70cc (Basler, Ahrensburg, Germany) with the GMAX3265 CMOS sensor, capable of delivering 70 frames per second with a 65 MP resolution (9344 × 7000 pixels). It is equipped with a macro lens, the Qioptiq Apo-Rodagon-D 2x 4/75 (Qioptiq/Excelitas, Göttingen, Germany). The camera was installed on motorised linear rails above the arena for X-Y translation, and its position was controlled using a joystick to keep the area of interest within the frame. The camera could be moved on the z-axis through a fine translation stage (Fig. S4). Acquiring videos at the camera's native full-sensor resolution (9344 × 7000 px; 65.4 MP) exceeded our data-throughput capacity: software compression was too slow and hardware compression introduced visible artifacts. We therefore recorded a square ROI covering ~25% of the sensor (3968 × 3968 px at 20 fps), corresponding to a 400 × 400 µm field of view (≈ 9.9 px/µm; 0.10 µm/px). This adjustment reduced the total image size but did not alter spatial sampling density, as the physical magnification and pixel size remained identical. This adjustment was not considered a significant loss of information, as the majority of the full frame was out of focus, due to the non-flat curvature of the animal's mantle.

Sedation

We used ethanol as a sedative during imaging. To achieve a state of sedation, the animal was gradually exposed to ethanol dissolved in artificial seawater, with the concentration incrementally increased up to 1.5%. The procedure was carried out in a large, dark bucket to reduce visual stimulation. This controlled approach minimised stress on the animal while ensuring effective sedation.

Ethanol is widely used in cephalopod research for its accessibility and reversibility (Andrews et al., 2013; Gleadall, 2013), but could in principle suppress neural activity or alter muscle responsiveness. In our dataset, however, PCA revealed near-identical component counts in sedated and awake head-fixed animals, and motor-unit size (in chromatophores) remained unchanged. Thus, ethanol neither artificially inflated nor suppressed the apparent number of motor subunits, validating its use as a non-invasive means to stabilize animals during high-speed recordings.

Marking procedure

Because the entire mantle of *Sepia* could not fit under the camera view, it was essential to consistently image the same skin region across recording sessions. To solve this issue we used Visible Implant Elastomer Tags (Northwest Marine Technology, Inc. n.d.), a small and practical silicon-based tagging method. To apply the tag, animals were anesthetised with 1.2 % ethanol and a drop of silicon-base tag was injected through a syringe in the skin (Fig. S5). The silicon was coupled with a curing agent and the tag solidified within 24 hours. This type of tag has been shown to be very effective in cephalopods (Barry et al., 2011; Brewer et al., 2012; Zeeh et al., 2009). In our case, the skin of both *Euprymna* and *Sepia* retained the tag for the entire lifespan and veterinarian analyses showed that the tagging did not cause any form of infection. A blue light lamp attached to the camera helped us find the tag by making it fluoresce. We then always filmed the area of skin around the same tag.

Head fixation

To enable long filming sessions, we utilised head fixation, allowing us to film a single area continuously with only minimal camera adjustments during recording (Fig. S6). Animals were transferred to a bucket containing 1.7% ethanol in ASW, and transferred to a shallow tank (1.5% ethanol in ASW, continuously bubbled with oxygen) at the onset of surgical plane anesthesia. The dorsal head was raised 1 cm above the water line by a silicone-coated head rest, and the gills were superfused with tank water at a rate of 60 ml/min via soft silicone tubes inserted bilaterally into the mantle cavity. Breathing rate was maintained by observation of the collar musculature and changes in ethanol concentration. Lidocaine (2%, 0.2ml) was injected subcutaneously before exposing the dorsal head cartilage, reapplying lidocaine and removing overlying connective tissue. A thin layer of Vetbond (3M) was then applied to the dorsal head cartilage before attaching a custom 3D-printed head plate (biocompatible resin) with dental cement (Venus, Kulzer) before sealing the wound with surgical glue and transferring the animal to a recovery tank.

Filming sessions

E. berryi: 14 animals were filmed. These recordings were used to establish experimental conditions and to develop and refine the analysis pipeline. To maximize spontaneous chromatophore activity, individuals were lightly sedated with 1–1.5% ethanol, which also induced slight chromatophore contraction. Expansion was triggered by cyclically varying the ambient light intensity with a custom, remotely controlled LED ring positioned above the arena, taking advantage of the light-dependent dynamics of chromatophores (Zylinski et al., 2011). Filming sessions varied in duration depending on the experimental condition. Sedated animals were recorded for up to 20 minutes before being returned to normal seawater for recovery, whereas non-sedated individuals could be filmed for up to 1 hour with continuous seawater circulation. Whenever possible, the same individuals were recorded every three days over the course of development, spanning a total period of approximately two months. The results presented here are based on recordings from a lightly sedated individual exposed to cyclic changes in ambient light intensity. This condition produced the most stable and interpretable chromatophore dynamics, minimizing motion artifacts while maintaining spontaneous activity.

S. officinalis: Over the course of the study, 12 individuals ranging in age from 5 days to 10 months post-hatching were filmed under various experimental conditions. A range of experimental configurations was explored to optimize chromatophore visibility and recording stability, including evoked camouflage using printed or e-ink patterns presented beneath a transparent tank, light ethanol sedation (up to 1.5 %), and head fixation. In selected individuals, the same skin region was imaged at three-day intervals for a maximum duration of six months. The dataset presented here was obtained from a head-fixed individual filmed on days 1, 2, and 6 post-surgery, both with and without light ethanol sedation. Head fixation provided stable, high-quality recordings with precise spatial correspondence between frames. Non-sedated sessions lasted up to

2 hours, while sedated sessions were limited to 20-minute bouts before recovery in normal seawater. Comparable results could be obtained from lightly sedated animals when movement was compensated by a tracking camera or other gentle immobilization.

Computational analyses

Chromatophore activity was quantified using the CHROMAS software package (Ukrow, Renard et al., 2025), which processes video data of cephalopod skin to identify individual chromatophores and extract their spatiotemporal dynamics. CHROMAS provides per-chromatophore metrics such as surface area, epicentre coordinates, and anisotropic deformation. The resulting dataset provided spatiotemporal maps of chromatophore activity, forming the basis for subsequent neural and biomechanical analyses. CHROMAS was used as described in Ukrow, Renard et al., 2025, with the following parameter and model choices.

For chunking, which filters out frames likely to impair analysis, we chose the difference-of-Gaussians (DoG) focus metric with kernel sizes k1=11, k2=5, and standard deviations s1=2 and s2=1 pixels.

To generate training data, manually annotated images (3968×3968 pixels) were divided into 512×512 pixel patches. Of these, 90% were randomly selected for training and the remaining 10% were held out for testing. To improve model generalisation, training data augmentation followed Ukrow, Renard et al., 2025 with the following parameters: spatial translations (±20%), scaling (±20%), rotation (±30°), RGB channel shifts (±25), brightness variation (±10%), contrast alteration (±30%), perspective warping (scale 0.05–0.5), and vertical/horizontal flipping. Each transformation was applied independently with a probability of 25%, except flipping, which was applied with a 50% probability.

Segmentation used the neural-network option of CHROMAS using a Fully Convolutional Network (FCN) architecture with a ResNet-50 backbone (Long et al., 2015). Training was performed for 500 epochs with validation every 5 epochs, using a composite loss function combining Dice loss and cross-entropy loss in equal proportion (50:50). Optimisation used the Adam optimiser with an initial learning rate of 0.001. A *ReduceLROnPlateau* scheduler (mode: ‘min’, factor: 0.1, patience: 50 epochs) adaptively reduced the learning rate when validation performance plateaued. The model with the lowest recorded validation error was retained for analysis.

For registration, 900 randomly selected tracking points were initialised on a 100×100 pixel grid. Displacement vectors exceeding 10 pixels were excluded. The interpolation parameter of the moving-least-squares algorithm was set to $\alpha = 3.0$.

For stitching, we applied the ellipse-fit option for *Euprymna berryi* and the manual option for *Sepia officinalis* as detailed in Ukrow & Renard, 2025. The interpolation parameter of the moving-least-squares algorithm was set to $\alpha = 3.0$.

All other parameters were set to their default values. To minimize analysis bias, the pipeline was fully automated and applied using identical parameters across all conditions and datasets.

Chromatophore anisotropic deformation tracking

Chromatophore anisotropic deformation tracking provides a detailed characterisation of the directional and irregular expansion patterns of chromatophores. This analysis begins with a stabilisation step that compensates for both global and local deformations of the skin. To achieve this, the CHROMAS pipeline identifies stable points on the skin, referred to as motion markers, which correspond to chromatophores that remain small and constant in size across frames. These motion markers are used to derive skin deformation over time, creating a stabilised coordinate system that eliminates artifacts caused by skin movement. Each chromatophore is divided into 36 radial slices to enable precise monitoring of its anisotropic deformations. This number of slices, determined based on the Nyquist–Shannon theorem (Shannon, 1948) and histological analysis (Fig. S7), was set to 36, corresponding to twice the upper bound of histologically confirmed muscle fibers. Using a higher resolution would mainly amplify small segmentation imperfections, the primary source of error. The epicenter of each chromatophore is used as the origin for radial

slicing and is calculated from the chromatophore's center of mass in its most contracted state. This epicenter remains stable across frames due to its relative positioning within the local coordinate system of motion markers. Slice areas are calculated by averaging distances from the epicenter to the chromatophore's edges, followed by squaring and scaling. This method ensures accuracy even in the presence of pixel discretization errors. Orientation of slices is maintained consistently across frames using the local coordinates derived from motion markers, allowing for the reliable tracking of individual slices over time.

Expansion and contraction speeds

We analyzed the expansion and contraction dynamics of chromatophores by tracking 36 radial slices for each of ten particularly active chromatophores. For each recording, area values were reshaped into a matrix of dimensions "number of frames × 36 slices" and converted to radii, assuming equal-angle sectors, using the relation r = sqrt(36 × area / π). Peak-centered events were defined for each slice after applying a light Savitzky–Golay smoothing (window size 5, polynomial order 2). Local maxima were detected on the smoothed radius traces using the *scipy.signal.find_peaks* function with a prominence threshold of 1.5. For each detected peak (at frame p), the onset of expansion was defined as the frame immediately before the first positive slope encountered when scanning left from the peak, and the end of contraction as the last frame with a negative slope when scanning right. Slopes were computed from the first difference of the radius signal, with a small threshold (epsilon = 1e-5) used to avoid spurious sign flips due to numerical jitter.

For each event, we calculated expansion amplitude ($A_{exp} = r_p - r_{start}$), duration ($D_{exp}$ = p − start), and mean speed ($S_{exp} = A_{exp} / D_{exp}$), as well as the corresponding contraction amplitude, duration, and speed ($A_{con} = r_p - r_{end}$, D_{con} = end − p, $S_{con} = A_{con} / D_{con}$). To suppress small fluctuations that likely represented noise, we excluded events with an expansion amplitude smaller than 15% of the full amplitude range. Events were then grouped by expansion amplitude into three categories based on percentile tails (tail width = 33%): "small" (lowest 33%), "center" (middle 33–67%), and "large" (highest 33%). Within each group, we applied Tukey's interquartile range (IQR) method to remove outliers based on both amplitude and speed, keeping only events that fell within [Q1 − k × IQR, Q3 + k × IQR], with k = 1.

Statistical comparisons of expansion versus contraction speeds and durations at the event level were performed using paired t-tests. Statistical significance was reported as follows: $p < 0.05$ (*), $p < 0.01$ (**), $p < 0.001$ (***), and $p < 0.0001$ (****). Durations were expressed in frames, equivalent to milliseconds when converted at 20 frames per second (e.g., 50 ms per frame).

Number and influence of motor neuron per chromatophore

To estimate the number of distinct motor neurons controlling each chromatophore, time series representing the expansion dynamics of radial slices were processed through a dimensionality reduction and source separation pipeline. Each chromatophore's area trace matrix (frames × slices) was first detrended using *scipy.signal.detrend*. Principal Component Analysis (PCA) was performed using *sklearn.decomposition*. PCA, and the number of meaningful components was estimated via the "elbow method", with the elbow point identified using the *kneed.KneeLocator* package (Satopaa, 2011). This number was then used as the n_components parameter for Independent Component Analysis (ICA), performed using *sklearn.decomposition.FastICA*. Initial ICA analyses showed that single components sometimes spanned both poles of a chromatophore, due to anticorrelated activity between opposing sides caused by the elastic mechanics of the pigment sacculus. To focus only on *active* motor signals, we filtered the data to retain only expansion events, resulting in independent components localized to one side and providing a clearer mapping of motor neuron influence.

The resulting ICA mixing matrix provides the contribution of each independent component to each radial slice. To quantify this influence, the absolute values of the mixing matrix were normalised per slice, yielding a percentage influence profile across components. These influence

profiles were visualised using polar plots to assess spatial distribution. The number of components (ICs) retained per chromatophore serves as an estimate of the number of distinct motor neuron inputs driving that chromatophore's expansion.

Number of chromatophores per motor unit

Motor units were inferred by clustering independent components (ICs) extracted from chromatophore activity traces using the FastICA algorithm (*sklearn.decomposition.FastICA*). To group ICs with similar temporal profiles, we applied Affinity Propagation (*sklearn.cluster.AffinityPropagation*) using pairwise Pearson correlation as the similarity metric. Each resulting cluster was interpreted as a putative motor unit, consisting of ICs presumed to originate from the same motor neuron. Chromatophores were then assigned to motor units based on their strongest IC loading. Motor unit size was defined as the number of unique chromatophores associated with each cluster. All steps were implemented in Python (*RRID:SCR_008394*) using *NumPy* (Harris et al., 2020) (*RRID:SCR_008633*), *pandas* (McKinney, 2010) (*RRID:SCR_018214*), and *scikit-learn* (Pedregosa et al., 2011) (*RRID:SCR_002577*).

Motor unit shape and structure

To characterize chromatophore clusters, we developed a Python script using *pandas* and *NumPy* for data handling, *SciPy* for distance calculations and minimum spanning tree construction, and *matplotlib* for visualization (Hunter, 2007) (*RRID:SCR_008624*). To assess the spatial distribution of chromatophores quantitatively, we computed nearest-neighbor distances (NND) using Python. Epicenter coordinates [epicenter_x, epicenter_y] were extracted from our dataset. For the global analysis, we computed pairwise Euclidean distances between all chromatophore epicenters and recorded the minimum distance to identify each chromatophore's nearest neighbor. For the within-cluster analysis, we grouped chromatophores by cluster label and repeated the NND computation within each group. The output metrics included the mean NND, standard deviation, and coefficient of variation (CV), which were used to describe both overall spatial density and intra-cluster compactness. Results were visualised by plotting chromatophore positions and connecting each to its nearest neighbor with a line segment. In addition to nearest-neighbor distances (NND), we calculated furthest-neighbor distances (FND) and convex hull areas (via *scipy.spatial.ConvexHull*) to estimate cluster extent. From these, density metrics were derived by relating chromatophore counts to convex hull area, and Pearson correlation coefficients (*scipy.stats*) were used to assess relationships between area, density, and number of chromatophores.

To visualize the putative motor units' ramifications, chromatophores were grouped by cluster label and plotted according to their epicenter coordinates, with multi-labeled chromatophores displayed as multicolored wedges, and internal cluster geometry was quantified by computing pairwise Euclidean distances and reducing them to a minimum spanning tree. This framework enabled both visualization and quantitative comparison of cluster compactness, extent, and density.

Second order innervation

To assess second-order innervation, we first extracted all combinations of chromatophore identifiers and their corresponding cluster labels from the dataset, yielding a unique set of cluster memberships. A pairwise co-occurrence count was computed by iterating over all clusters and recording how often each pair of chromatophores appeared together; we then counted how many pairs occurred together in two or more clusters. For the null model, we implemented a constrained permutation in which chromatophore IDs were randomly reassigned across clusters while preserving the number of unique IDs per cluster. This procedure maintains the original cluster sizes but not the per-chromatophore memberships. Across 1,000 simulations, we repeated

the pairwise counting procedure and recorded the number of pairings that reached the second-order threshold. This produced a distribution of null values, against which the real count was compared using a two-tailed z-test to determine statistical significance.

Electrophysiology

Animals

Electrophysiological experiments were carried out in Beijing, China. At the time of the experiments, there were no specific national regulations governing the use of cephalopods in research in China. Nevertheless, all procedures performed at Peking University were designed to comply, as far as possible, with the principles of the European Directive 2010/63/EU and FELASA recommendations.

For electrophysiological experiments, bobtail squids *Euprymna berryi* were either hatched from eggs laid in house or purchased as eggs and naturally hatched in the lab. Both adult squids and eggs were sourced from Guangdong and Hainan provinces in China. *E. berryi* were reared in an artificial seawater (ASW) system around 24 °C, with a salinity of 28 ppt and a pH of 8.3. Water quality was monitored continuously and was tested regularly. The ASW filtration system consists of filter floss, filter bags, biofilter (for nitrifying bacteria), a protein skimmer, and UV-lamp. Room light was set as a 12h-12h light-dark cycle with gradual on- and off-sets at 12:00 and 24:00.

Brain and skin preparation

Juvenile *E. berryi* ranging from 5-10 mm in body length were used for electrophysiological experiments. Animals were first anesthetized by 2% ethanol in ASW, and then transferred into an acrylic chamber with a sloped silicone rubber base, filled with oxygenized calcium-free saline (460 mM NaCl, 10 mM KCl, 10 mM glucose, 10 mM HEPES, 55 mM $MgCl_2$, and with a pH of 7.4.) at room temperature. The arms, beak, and both eyes were removed. The mantle was opened from the ventral side and all visceral organs were removed. The skin of the head was removed to expose the posterior sub-esophageal mass. The posterior chromatophore lobe was de-sheathed gently with fine forceps. The mantle was pinned on a 70° sloped silicone rubber plane, while the brain was placed on a flat silicone rubber base. The mantle and the brain were connected solely through pallial nerves. The solution was then replaced by oxygenated (100% O2) calcium-containing saline (460 mM NaCl, 10 mM KCl, 10 mM glucose, 10 mM HEPES, 55 mM $MgCl_2$, 11 mM $CaCl_2$, and with a pH of 7.4).

Electrophysiological recording and imaging setup

The patch clamp recording was performed under an upright fluorescence microscope (BX51W1, Olympus, Tokyo, Japan) with a 20 water-immersion objective (UMPlanFI 20, Olympus, Tokyo, Japan). The brain was visualized using a microscope camera (Moment, Teledyne Vision Solutions, Thousand Oaks, California, USA). The mantle chromatophore was recorded using a camera (a2A4096-30ucBAS, Basler, Ahrensburg, Germany) with a manual lens (MLM-3X-MP, Computar, Tokyo, Japan) at 30 fps. The glass electrodes (~8 M) were made from borosilicate glass (BF150-86-10, WPI, Sarasota, Florida, USA) by a puller (P-1000, Sutter Instrument, Novato, California, USA). The pipettes were filled with internal solution (450 mM K-gluconate, 10 mM NaCl, 4 mM $MgCl_2$, 3 mM EGTA, 20 mM HEPES, 2 mM Mg-ATP, 0.2 mM Na-GTP, 2% neurobiotin, and with pH of 7.4). Recordings were performed in current clamp mode with a HEKA amplifier (ESC100-USB, Lambrecht, Germany). For intracellular stimulation, step or constant currents were injected repetitively at 0.5 Hz. The onset of the stimulation train simultaneously triggered the camera to record chromatophore activity on the mantle skin.

Supplementary figures

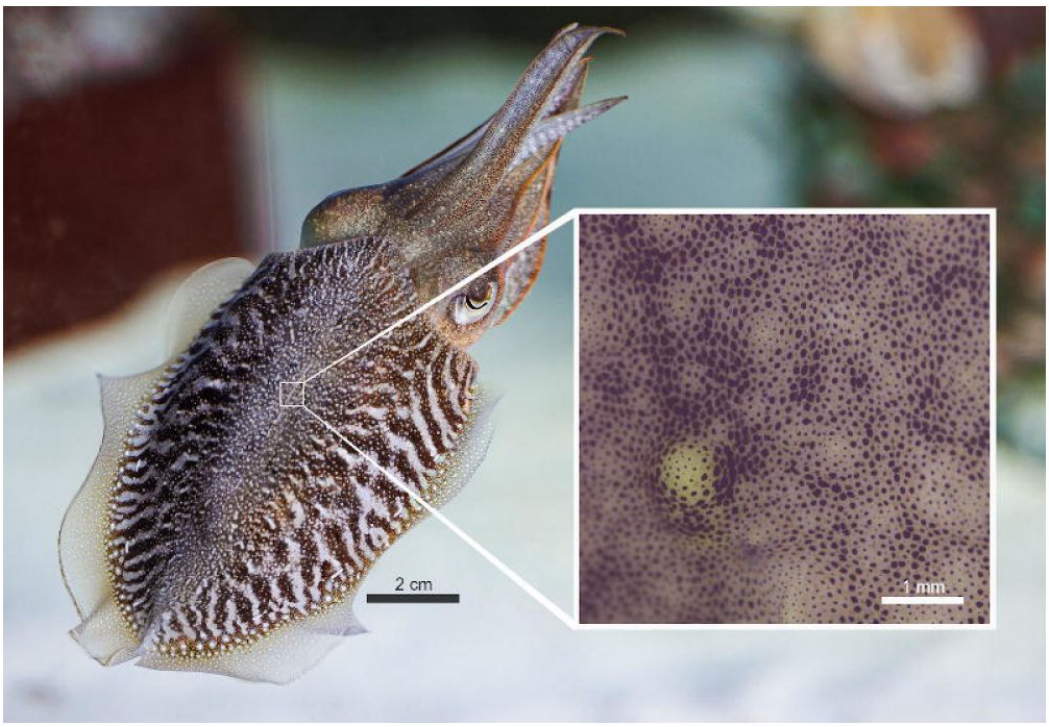

Figure S1. ***Sepia officinalis*** **(mantle length 20 cm; photograph by Stephan Junek, Max Planck Institute for Brain Research).** The inset shows the analyzed region of interest at the center of the mantle (0.5 × 0.5 cm).

Figure S2. Relative temporal composition of chromatophore events across amplitude groups.

For each amplitude category (SMALL, MEDIUM, LARGE), the proportion of frames spent in the expansion (green) versus contraction (red) phase was computed across all valid events (n = 2157). Percentages were calculated relative to the total duration of each event (expansion + contraction). This analysis corresponds to the same dataset shown in Fig. 5.

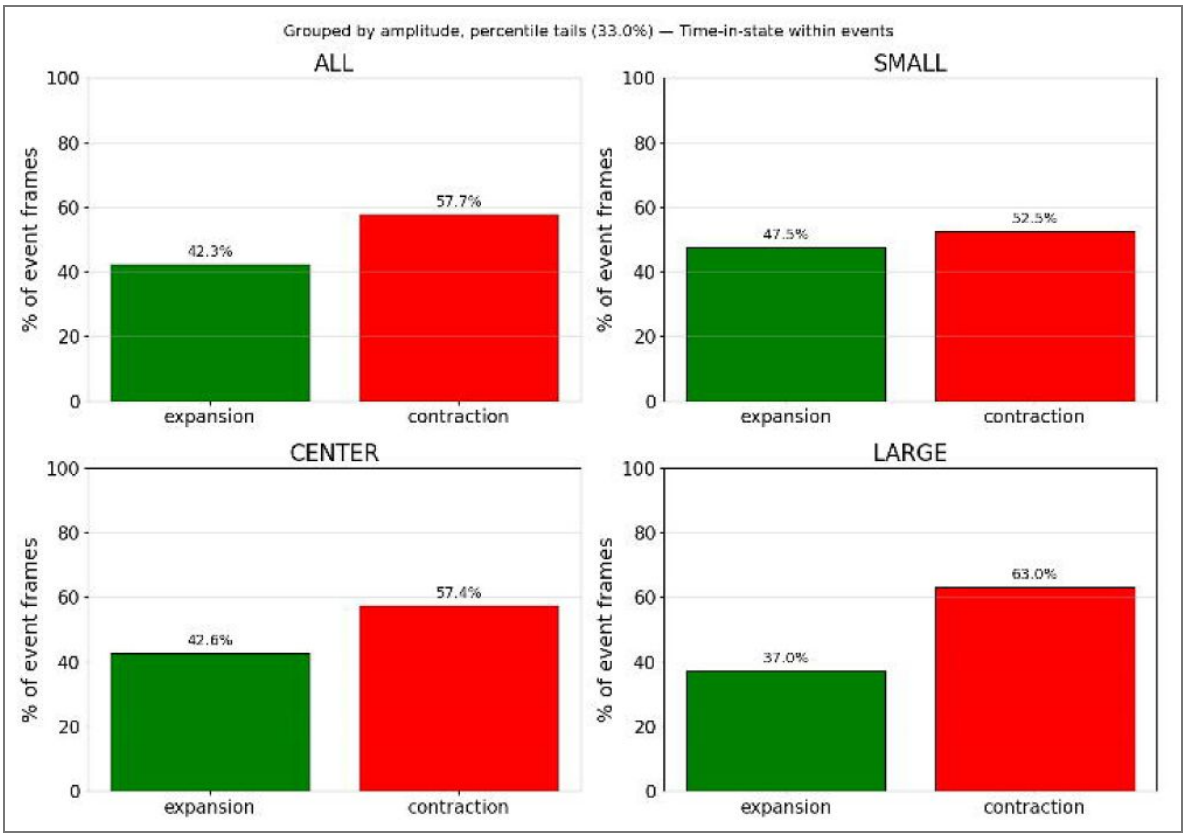

Figure S3. Designs of experimental arenas.

a) Arena for *Euprymna berryi* hatchlings. b) Rig for *Sepia officinalis*. Four adjustable LED lamps in yellow. Transparent tank in cyan. Structure in gray.

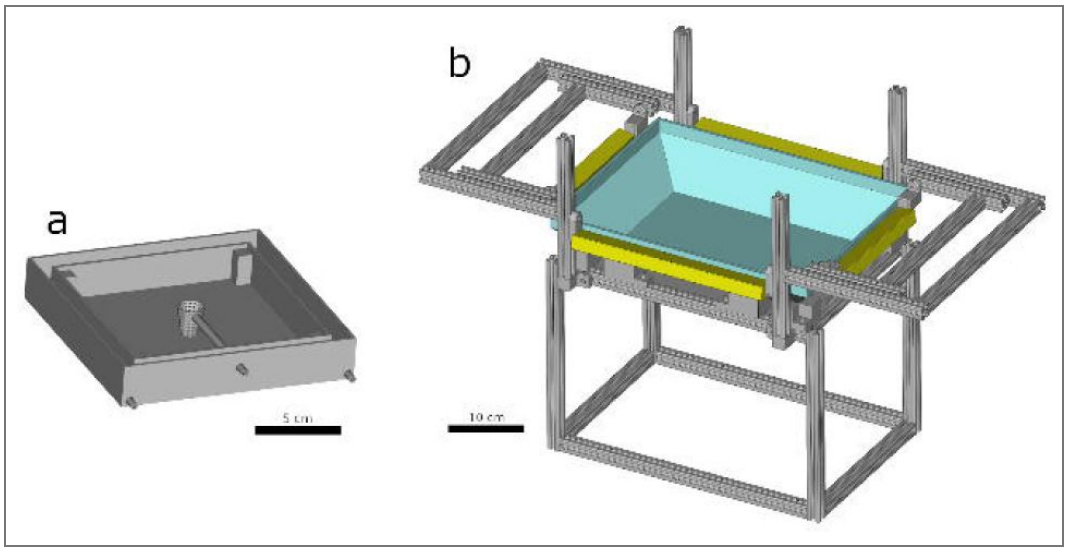

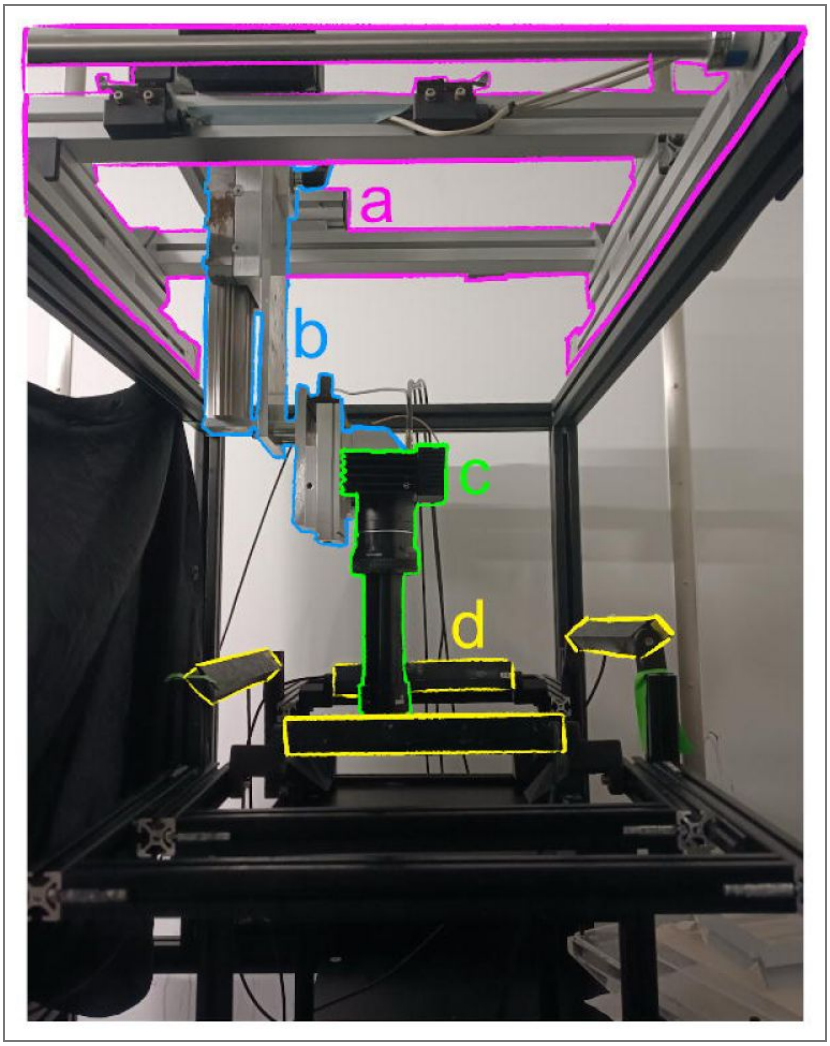

Figure S4. Sepia filming setup.

a) Remotely controlled linear rails. b) Z-axis manual translation stage. c) Camera and lens. d) LED lights.

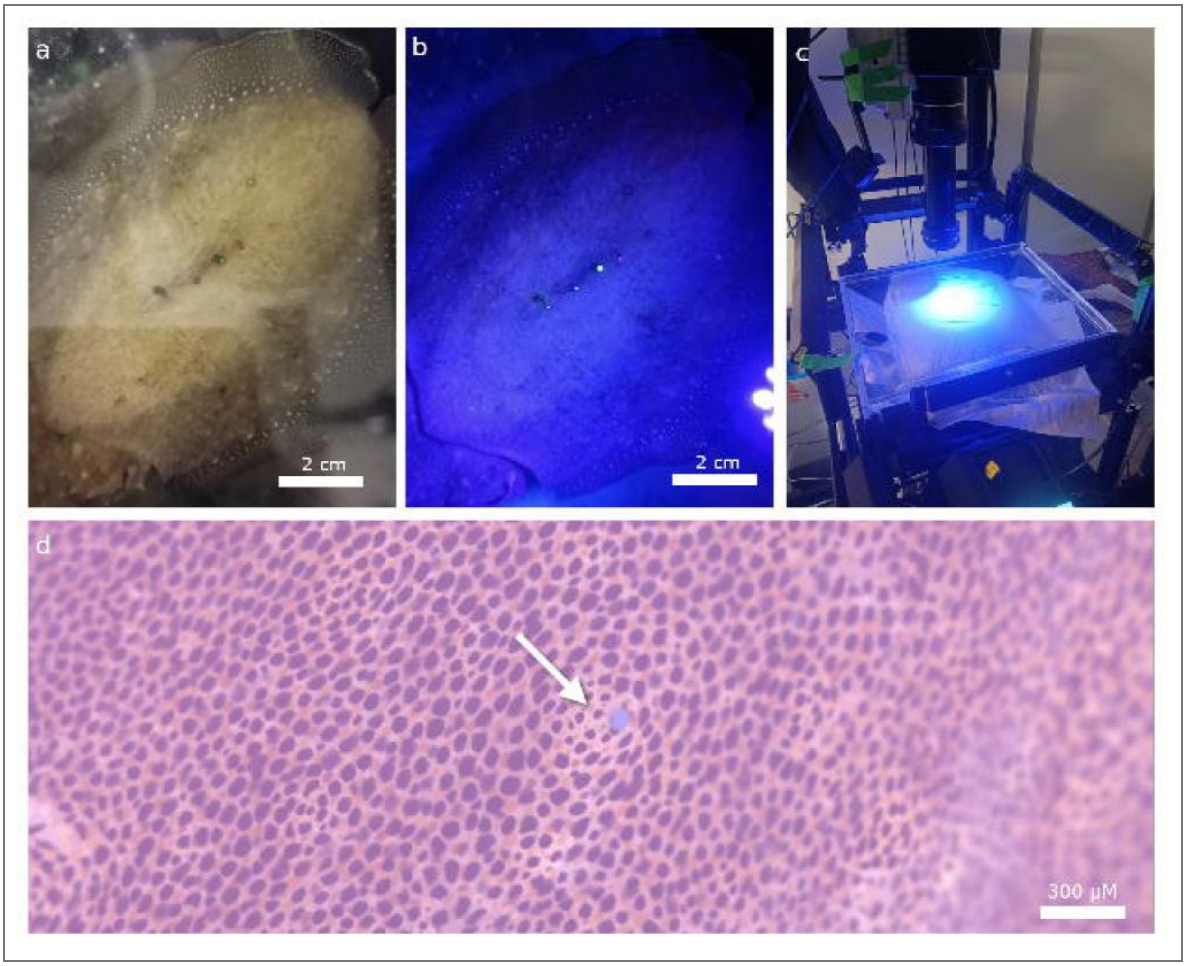

Figure S5. Visible implant elastomer tagging.

a) Sepia officinalis marked at the center of the mantle with tags of various colors in a row. b) Marked animal under fluorescent light. c) Fluorescent lamp mounted next to the camera on the filming rig. d) Footage captured by the high-resolution camera. Close-up on the blue fluorescent tag indicated by an arrow.

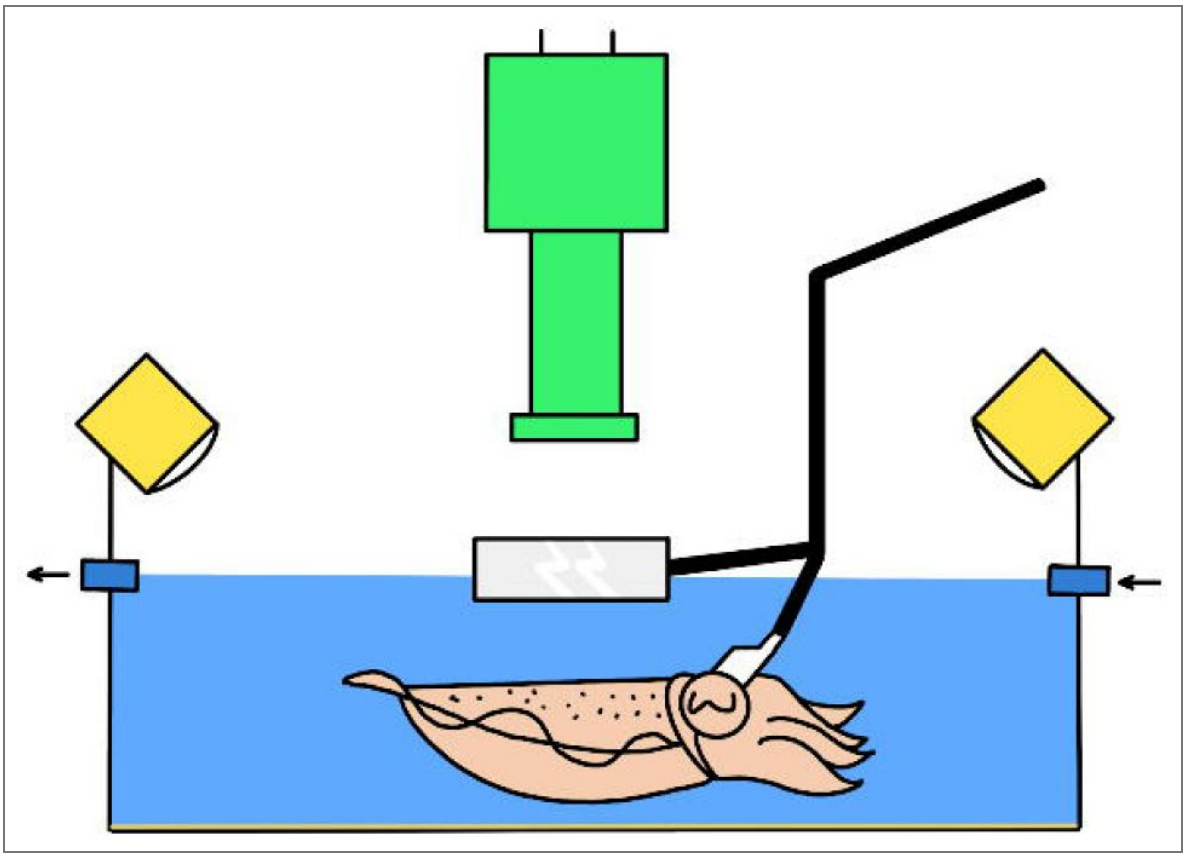

Figure S6. Schematics of experimental setup with head fixation.

The camera (green) is positioned above the tank, which is filled with artificial seawater (blue). A constant flow of water (indicated by arrows) ensures proper oxygenation. LEDs (yellow) surrounding the tank provide uniform illumination. A bracket (black) supports a thick glass panel (gray) to minimize water distortion during filming. The same bracket also holds a head-fixation mount (white) to stabilize the animal's head.

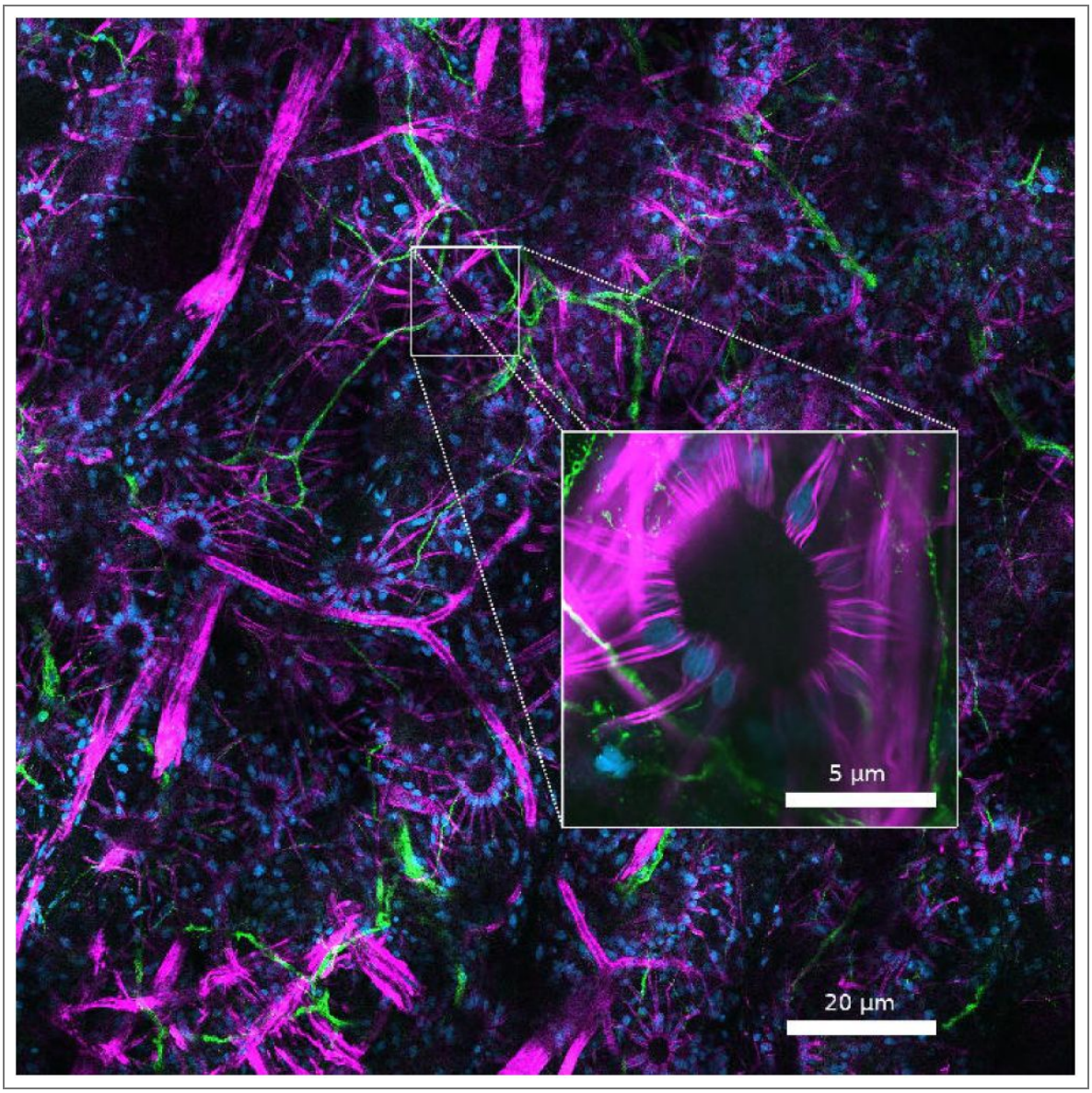

Figure S7. Confocal image of *E. berryi*'s stained skin captured with ZEISS LSM 980.

DAPI in blue (nuclei), phalloidin in magenta (muscle fibers), and tubulin in green (nerve fibers). A single chromatophore is highlighted (white box) to illustrate its cellular organization. Radial muscle fibers (magenta) extend outward from the central pigment sacculus, with nuclei (blue) arranged in a rosette at the base of each fiber. Tubulin-labeled nerve fibers (green) approach the muscles, suggesting potential neuromuscular connections, though the precise contact points cannot be confirmed in the absence of a neuromuscular junction marker.

Data availability

The image analysis software CHROMAS is distributed via the pypi package index (*https://pypi.org/project/chromas/*) and is publicly released on GitLab (*https://doi.org/10.17617/1.pa38-mh49*) under the 3-Clause BSD License. The documentation is hosted on GitLab. The data used to train the segmentation models, the trained models, and example videos for the tutorial can be found at *https://public.brain.mpg.de/Laurent/Chromas2025*. Electrophysiology videos and trace data are provided in a separate folder named "ephys".

Acknowledgements

We thank F. Bayer for assistance in building the experimental setup; F. Kretschmer for optimizing the camera control, recording software and Git workflows; F. Vollrath and S. Junek for help with image acquisition; P. Musset for help with high performance computing; L. Jürgens, S. Schwind, L. E. Reyes de Frey, D. Burgard, M. Landler, M. Minde, S. Kranz, P. Dominiczak, N. K. Vogt, G. Wexel, S. Dizdarevic and E. Northrup for animal care; and T. Woo and other members of the Laurent laboratory for constructive exchanges. We thank Alice Perenzin and Antje Berken for grant management and scientific coordination. This research was funded by the Max Planck Society (GL), by the LOEWE Schwerpunkt CMMS (State of Hesse) (GL), by the Louis Jeantet Foundation (GL), by the European Union (ERC grant CAMOUFLAGE, 10114150) (GL), by National Natural Science Foundation of China (NSFC grant 32371215) (XL), State Key Laboratory of Membrane Biology, Peking University (XL); and Peking-Tsinghua Center for Life Sciences (XL).

Additional files

Supplemental movie 1. Video example of patch clamp stimulation. On the left, a video showing the expansion of five chromatophores composing a motor unit—the same motor unit shown in 6b. On the right, membrane-potential trace from the corresponding motor neuron, synchronized with the video on the left.

Additional information

Funding

Funder	Grant reference number	Author
Max Planck Society		Gilles Laurent
EC | European Research Council (ERC)	ERC grant CAMOUFLAGE 10114150	Gilles Laurent
Louis-Jeantet Foundation		Gilles Laurent
MOST | National Natural Science Foundation of China (NSFC)	32371215	Xitong Liang
State Key Laboratory of Membrane Biology, Peking University		Xitong Liang
Peking-Tsinghua Center for Life Sciences		Xitong Liang

Author ORCID iDs

Gilles Laurent: https://orcid.org/0000-0002-2296-114X

References

Andrews P. L., Darmaillacq A., Dennison N., Gleadall I. G., Hawkins P., Messenger J. B., Osorio D., Smith V. J., Smith J. A (2013) The identification and management of pain, suffering and distress in cephalopods, including anaesthesia, analgesia and humane killing. *Journal of Experimental Marine Biology and Ecology* **447**:46-64 https://doi.org/10.1016/j.jembe.2013.02.010

Asensio-Montesinos F., Blaya-Valencia G., Corbí H., Beltrán-Sanahuja A., Sanz-Lázaro C (2022) Microplastic accumulation dynamics in two Mediterranean beaches with contrasting inputs. *Journal of Sea Research* **188**:102269 https://doi.org/10.1016/j.seares.2022.102269

Atwood H. L (1977) Crustacean neuromuscular systems: past, present, and future. In: Hoyle G. L (Ed). *Identified neurons and behavior of arthropods* Boston, MA: Springer US. pp. 9-29 https://doi.org/10.1007/978-1-4684-6967-7_2

Barry P. D., Tamone S. L., Tallmon D. A (2011) A comparison of tagging methodology for North Pacific giant octopus Enteroctopus dofleini. *Fisheries Research* **109**:370-372 https://doi.org/10.1016/j.fishres.2011.02.011

Bettoso N., Borme D., Faresi L., Aleffi I., Orlando-Bonaca M., Lipej L (2016) New insights on the biological parameters of the exploited cuttlefish Sepia officinalis L.(Mollusca: Cephalopoda) in the northern Adriatic Sea in relation to the main fishing gears employed. *Mediterranean Marine Science* **17**:152-162 https://doi.org/10.12681/mms.1311

Blott S. J., Pye K (2012) Particle size scales and classification of sediment types based on particle size distributions: Review and recommended procedures. *Sedimentology* **59**:2071-2096 https://doi.org/10.1111/j.1365-3091.2012.01335.x

Boycott B. B (1961) The functional organization of the brain of the cuttlefish Sepia officinalis. *Proceedings of the Royal Society of London. Series B, Biological Sciences* **153**:503-534 https://doi.org/10.1098/rspb.1961.0015

Brewer R. S., Norcross B. L (2012) Long-term retention of internal elastomer tags in a wild population of North Pacific giant octopus (Enteroctopus dofleini). *Fisheries Research* **134**:17-20 https://doi.org/10.1016/j.fishres.2012.07.020

Bullock T., Horridge G. A (1965) *Structure and function in the nervous systems of invertebrates* W. H. Freeman and Company.

Campello R. J. G. B., Moulavi D., Sander J. (2013) Density-Based Clustering Based on Hierarchical Density Estimates. In: Pei J., Tseng V. S., Cao L., Motoda H., Xu G. (Eds). *Advances in Knowledge Discovery and Data Mining* Springer. pp. 160-172 https://doi.org/10.1007/978-3-642-37456-2_14

Cloney R. A., Florey E (1968) Ultrastructure of cephalopod chromatophore organs. *Zeitschrift Für Zellforschung Und Mikroskopische Anatomie* **89**:250-280 https://doi.org/10.1007/BF00347297 | PubMed

Dauvin J. C., Bakalem A., Baffreau A., Delecrin C., Bellan G., Lardicci C., ..., Grimes S. (2017) The well sorted fine sand community from the western Mediterranean Sea: A resistant and resilient marine habitat under diverse human pressures. *Environmental pollution* **224**:336-351 https://doi.org/10.1016/j.envpol.2017.02.013 | PubMed

Dubas F., Boyle P. R (1985) Chromatophore motor units in Eledone cirrhosa (Cephalopoda: Octopoda). *Journal of experimental biology* **117**:415-431 https://doi.org/10.1242/jeb.117.1.415

Dubas F.., Hanlon R. T., Ferguson G. P., Pinsker H. M (1986) Localization and stimulation of chromatophore motor neurones in the brain of the squid, Lolliguncula brevis. *Journal of Experimental Biology* **121**:1-25 https://doi.org/10.1242/jeb.121.1.1 | PubMed

Florey E (1969) Ultrastructure and function of cephalopod chromatophores. *American Zoologist* **9**:429-442 https://doi.org/10.1093/icb/9.2.429 | PubMed

Gleadall I. G (2013) The effects of prospective anaesthetic substances on cephalopods: summary of original data and a brief review of studies over the last two decades. *Journal of Experimental Marine Biology and Ecology* **447**:23-30 https://doi.org/10.1016/j.jembe.2013.02.008

Hanlon R. T., Messenger J. B (1988) Adaptive coloration in young cuttlefish (Sepia officinalis L.): the morphology and development of body patterns and their relation to behaviour. Philosophical Transactions of the Royal Society of London. B. *Biological Sciences* **320**:437-487 https://doi.org/10.1098/rstb.1988.0087

Harris C. R., Millman K. J., Van Der Walt S. J., Gommers R., Virtanen P., Cournapeau D., Wieser E., Taylor J., Berg S., Smith N. J., *et al.* (2020) Array programming with NumPy. *Nature* **585**:357-362 https://doi.org/10.1038/s41586-020-2649-2 | PubMed

Henneman E (1957) Relation between Size of Neurons and Their Susceptibility to Discharge. *Science* **126**:1345-1347 https://doi.org/10.1126/science.126.3287.1345

Hoyle G (1955) The anatomy and innervation of locust skeletal muscle. *Proceedings of the Royal Society of London. Series B-Biological Sciences* **143**:281-292 https://doi.org/10.1098/rspb.1955.0011 | PubMed

How M. J., Norman M. D., Finn J., Chung W. S., Marshall N. J (2017) Dynamic skin patterns in cephalopods. *Frontiers in physiology* **8**:393 https://doi.org/10.3389/fphys.2017.00393 | PubMed

Hunter J. D (2007) Matplotlib: A 2D graphics environment. *Computing in science & engineering* **9**:90-95 https://doi.org/10.1109/MCSE.2007.55

Kernell D (2006) *The Motoneurone and its Muscle Fibres* Oxford University Press. https://doi.org/10.1093/acprof:oso/9780198526551.001.0001

Laan A., Gutnick T., Kuba M. J., Laurent G (2014) Behavioral analysis of cuttlefish traveling waves and its implications for neural control. *Current biology* **24**:1737-1742 https://doi.org/10.1016/j.cub.2014.06.027 | PubMed

Long J., Shelhamer E., Darrell T. (2015) Fully convolutional networks for semantic segmentation. In: Proceedings of the IEEE conference on computer vision and pattern recognition. pp. 3431-3440 https://doi.org/10.1109/TPAMI.2016.2572683

Lucas B. D., Kanade T (1981) An Iterative Image Registration Technique with an Application to Stereo Vision. In: IJCAI'81: 7th International Joint Conference on Artificial Intelligence. **2** pp. 674-679 https://hal.science/hal-03697340

McKinney W (2010) Data Structures for Statistical Computing in Python. *Scipy* https://doi.org/10.25080/Majora-92bf1922-00a

Masland R. H (2012) The neuronal organization of the retina. *Neuron* **76**:266-280 https://doi.org/10.1016/j.neuron.2012.10.002 | PubMed

Mather J. A., Mather D. L (2004) Apparent movement in a visual display: the 'passing cloud' of Octopus cyanea (Mollusca: Cephalopoda). *Journal of Zoology* **263**:89-94 https://doi.org/10.1017/S0952836904004911

Messenger J. B (2001) Cephalopod chromatophores: neurobiology and natural history. *Biological Reviews* **76**:473-528 https://doi.org/10.1017/S1464793101005772 | PubMed

Mountcastle V. B (2005) *The sensory hand: neural mechanisms of somatic sensation* Harvard University Press.

Northwest Marine Technology (2024) Visible implant elastomer. https://www.nmt.us/visible-implant-elastomer/

Packard A (1982) Morphogenesis of chromatophore patterns in cephalopods: are morphological and physiological units the same?. *Malacologia* **23**:193-201

Pedregosa F., Varoquaux G., Gramfort A., Michel V., Thirion B., Grisel O., ..., Duchesnay É. (2011) Scikit-learn: Machine learning in Python. *The Journal of machine Learning research* **12**:2825-2830

Reiter S., Hülsdunk P., Woo T., Lauterbach M. A., Eberle J. S., Akay L. A., Longo A., Meier-Credo J., Kretschmer F., Langer J. D., *et al.* (2018) Elucidating the control and development of skin patterning in cuttlefish. *Nature* **562**:361-366 https://doi.org/10.1038/s41586-018-0591-3 | PubMed

Sandulli R., De Leonardis C., Vanaverbeke J. (2010) Meiobenthic communities in the shallow subtidal of three Italian Marine Protected Areas. *Italian Journal of Zoology* **77**:186-196 https://doi.org/10.1080/11250000903476616

Sasaki K., Burrows M (1998) Innervation pattern of a pool of nine excitatory motor neurons in the flexor tibiae muscle of a locust hind leg. *Journal of experimental biology* **201**:1885-1893 https://doi.org/10.1242/jeb.201.12.1885 | PubMed

Satopaa V., Albrecht J., Irwin D., Raghavan B. (2011) Finding a "Kneedle" in a Haystack: Detecting Knee Points in System Behavior. In: 31st international conference on distributed computing systems workshops. pp. 166-171 https://doi.org/10.1109/ICDCSW.2011.20

Shannon C. E (1948) A mathematical theory of communication. *The Bell System Technical Journal* **27**:379-423 https://doi.org/10.1002/j.1538-7305.1948.tb01338.x

Ukrow J., Renard M. D., Moghimi M., Laurent G (2025) A computational pipeline to track chromatophores and analyze their dynamics. *eLife* **14**:RP106509 https://doi.org/10.7554/eLife.106509.3

Wentworth C. K (1922) A scale of grade and class terms for clastic sediments. *The journal of geology* **30**:377-392 https://doi.org/10.1086/622910

Zylinski S., Johnsen S (2011) Mesopelagic cephalopods switch between transparency and pigmentation to optimize camouflage in the deep. *Current Biology* **21**:1937-1941 https://doi.org/10.1016/j.cub.2011.10.014 | PubMed

Zeeh K. M., Wood J. B (2009) Impact of visible implant elastomer tags on the growth rate of captive Caribbean reef squid Sepioteuthis sepioidea. *Fisheries Research* **95**:362-364 https://doi.org/10.1016/j.fishres.2008.08.002

Peer reviews

Reviewer #1 (Public review):

Renard, Ukrow et al. applied their recently published computational pipeline (CHROMAS) to the skin of Euprymna berryi and Sepia officinalis to track the dynamics of cephalopod chromatophore expansion. By segmenting each chromatophore into radial slices, and analyzing the co-expansion of slices across regions of the skin, they inferred the motor control underlying chromatophore groups.

Strengths:

- The authors demonstrate that most motor units of cephalopod skin include a subregion of multiple chromatophores, creating "virtual chromatophores" between fixed chromatophores. This is an interesting concept that challenges prevailing models of chromatophore organization, and raises interesting possibilities for how chromatophore arrays may be patterned during development.

- This study introduces new analytical approaches of cephalopod skin that will be valuable for the quantitative study of cephalopod behavior.

Weaknesses:

- The authors use patch-clamp experiments in E. berryi to test their approach for inferring motor units. The stimulations indeed evoke expansions of sub-regions of each chromatophore, creating "virtual chromatophores". However, they were not able to predict these motor units from behavioral analysis before confirming them with patch-clamp, limiting the strength of this validation.

- In S. officinalis, chromatophores are far more numerous than in E. berryi and exhibit frequent spontaneous activity, making it more challenging to distinguish shared motor drive.

Patch-clamp experiments in this species would provide important validation and strengthen confidence in the method for inferring motor units.

- Although multiple experimental conditions were tested (e.g., age, size, behavioral context, sedation, head-fixation, lighting), data is only shown from a small subset of experiments. Analyzing pooled data across conditions would allow for more generalizable conclusions.

- Different clustering algorithms were used for the two species (HDBSCAN for E. berryi and Affinity Propagation for S. officinalis). Since Affinity Propagation appeared to better capture correlation structure in S. officinalis, it would be informative to reanalyze the E. berryi data using the same method to assess potential algorithm-dependent biases.

Conclusion:

The CHROMAS tool is likely to be valuable to the field, given the need for quantitative frameworks in cephalopod biology. The predictions outlined here provide a useful foundation for future experimental investigation.

https://doi.org/10.7554/eLife.110074.2.sa3

Reviewer #2 (Public review):

Summary:

Overall, this is an excellent paper, making use of a newly developed system for monitoring the behaviour of chromatophores in the skin of (mostly) free swimming bobtail squid and European cuttlefish. The manuscript is very well written, clearly presented and very well structured. The central finding, that individual chromatophores are connected to multiple motor neurones, is not new. Novelty instead comes from the ability to measure the actuation of chromatophore sections across wide areas of skin in free-swimming animals, showing the diversity of local motor units and reinforcing the notion that individual chromatophores are not necessarily the individual units of colour change, but rather local motor units that cover multiple neighbour and near neighbour chromatophore muscles. This is an excellent finding and one that will shape our understanding of the neural control of cephalopod skin colour. I have a number of minor points below that the authors will need to address before acceptance.

Strengths:

The methodological approach to collecting large amounts of data about local variations in the expansion of sections of chromatophores is exciting, and the analysis pipeline for clustering sections of chromatophores whose spontaneous activity correlated over time is powerful and exciting.

Comments on revisions:

All concerns have been addressed in the revised version of the manuscript.

https://doi.org/10.7554/eLife.110074.2.sa2

Reviewer #3 (Public review):

Summary:

This study uses high-resolution videography and a custom computer-vision pipeline to dissect the motor control of cephalopod chromatophores in Euprymna berryi and Sepia officinalis. By quantifying anisotropic chromatophore deformations and applying dimensionality

reduction methods, the authors infer that individual chromatophores can be a part of multiple motor units. Clustering analyses reveal putative motor units that often span multiple chromatophores, with diverse and overlapping geometries. Chromatophore expansion dynamics are faster and more stereotyped than relaxation, consistent with active neural contraction followed by passive recoil. Together, the results show that chromatophores function not as uniform pixels but as fractionated, coordinately controlled elements that enable flexible pattern generation

Strengths:

The authors present compelling, direct evidence that a). chromatophore deformations are anisotropic, and indirect evidence that b). individual chromatophores can be split across multiple putative motor units. This evidence is provided through data collected over large spatial scales, but also at a sub-chromatophore resolution. This combination of scale and resolution is not possible using traditional neuroanatomical and physiological approaches alone.

The authors also develop a new non-invasive, image analysis approach to extract information about chromatophore deformation across large spatial scales on the organism's body. In principle this approach is applicable across species and may allow for further comparative characterization of chromatophore motor control. It is therefore a promising new tool and useful resource for the community.

Weaknesses:

An important weakness of the work is that the methods the authors develop can only be applied during resting, spontaneous 'flickering' activity of chromatophores to yield interpretable results at the motor unit level. This is because common presynaptic input would confound the identification of individual motor units. Thus, there remains a large difficulty in linking insights about single motor unit organization to the circuit and behavioral levels.

Another weakness of this paper is the rather limited electrophysiological validation of the computational findings. The authors present only one electrophysiology experiment in E. berryi, the species that they used only for 'methodological development' and not for detailed characterization. A complementary electrophysiological experiment in S. officinalis, or some visualization of neuron morphology confirming that motor neurons do indeed project to multiple chromatophores would strengthen the generalizability of their computational analysis. This would be particularly pertinent to validate the author's claim that some motor units contain chromatophores that are quite distant from one another on the animal.

Overall, the authors' technical contributions and method development are an important advance. This work serves as an excellent proof of concept that their method can extract useful information about chromatophore motor control. Further validation of their method is needed to fully trust the fine-scale conclusions drawn about the distribution and composition of multi-innervated chromatophores. Furthermore, the authors raise many interesting ideas about developmental constraints on circuit wiring and potential adaptive significance of multi-innervated chromatophores for certain features of camouflage patterning. Their method may be able to help resolve some of these questions in the future if it is refined and applied across developmental stages, regions on the animal, and across species

Comments on revisions:

Thank you for clarifying my major point of confusion regarding how one might connect these results to behaviorally relevant camouflage. I now have a better understanding of the author's rationale in studying resting activity of motor units and believe that the

clarifications added to the manuscript will help other readers who encounter similar confusion.

https://doi.org/10.7554/eLife.110074.2.sa1

Author response:

The following is the authors' response to the original reviews.

> ***Public Reviews:***
>
> ***Reviewer #1 (Public review):***
>
> *Summary:*
>
> *Renard, Ukrow et al. applied their recently published computational pipeline (CHROMAS) to the skin of Euprymna berryi and Sepia officinalis to track the dynamics of cephalopod chromatophore expansion. By segmenting each chromatophore into radial slices and analyzing the co-expansion of slices across regions of the skin, they inferred the motor control underlying chromatophore groups.*
>
> *Strengths:*
>
> *The authors demonstrate that most motor units of cephalopod skin include a subregion of multiple chromatophores, creating "virtual chromatophores" in between the fixed chromatophores. This is an interesting concept that challenges prevailing models of chromatophore organization, and raises interesting possibilities for how chromatophore arrays may be patterned during development.*
>
> *This study introduces new analyses of cephalopod skin that will be valuable for the quantitative study of cephalopod behavior.*
>
> *Weaknesses:*
>
> *The authors chose to image spontaneous skin changes in sedated animals, rather than visually-evoked skin changes in awake, freely-moving animals. Spontaneous chromatophore changes tend to be small shimmers of expansion and contraction, rather than obvious, sizable expansions. This may make it more challenging to distinguish truly co-occurring expansions from background activity. The authors don't provide any raw data (videos) of the skin, so it is difficult to independently assess the robustness of the inferred chromatophore groupings.*
>
> *The patch-clamp experiments in E. berryi are used to test the validity of their approach for inferring motor units. The stimulations evoke expansions of sub-regions of each chromatophore, creating "virtual chromatophores" as predicted from the behavioral analysis. However, the authors were not able to predict these specific motor units from behavioral analysis before confirming them with patch-clamp, limiting the strength of the validation. It would be informative to quantify the results of the patch-clamp experiments - are the inferred motor units of similar sizes to those predicted from behavior?*
>
> *The authors report testing multiple experimental conditions (e.g., age, size, behavioral stimuli, sedation, head-fixation, and lighting), but only a small subset of these data are presented. It is difficult to determine which conditions were used for which experiments, and the manuscript would benefit from pooling data from multiple experiments to draw general conclusions about the motor control of cephalopod skin.*

> *The authors use a different clustering algorithm for E. berryi and S. officinalis, but do not discuss why different clustering approaches were required for the two species.*
>
> *Impact:*
>
> *The authors use their computational pipeline to generate a number of interesting predictions about chromatophore control, including motor unit size, their spatial distribution within the skin, and the independent control of subregions within individual chromatophores by putatively distinct motor neurons. While these observations are interesting, the current data do not yet fully support them.*
>
> *The CHROMAS tool is likely to be valuable to the field, given the need for quantitative frameworks in cephalopod biology. The predictions outlined here provide a useful foundation for future experimental investigation.*

We thank the reviewer for the thoughtful and detailed evaluation of our work and for recognizing the potential of the CHROMAS pipeline for studying chromatophore control.

We agree that some aspects of the manuscript required clarification and additional explanation, and we have revised the text accordingly. We also now provide access to representative raw video recordings in the Data Availability section. In the *E. berryi* patch-clamp experiments, single motor neurons evoked expansions of sub-regions of chromatophores, consistent with the "virtual chromatophore" concept. We have now quantified the size of motor units across patch-clamp sessions, and the results show that the inferred motor-unit sizes broadly match those predicted from behavioral recordings, supporting the validity of our approach.

We agree that pooling data across individuals would provide valuable insight into variability across animals. In practice, we recorded chromatophore activity from several animals (14 *Euprymna berryi* and 12 *Sepia officinalis*) under different experimental conditions during development of the experimental pipeline. However, acquiring long, stable, artifact-free recordings suitable for motor unit analysis is technically challenging. We now clarify this point in the manuscript. Specifically, we explain that multiple animals were recorded during pipeline development, while the analyses presented focus on recordings with the highest signal quality. We anticipate that the framework introduced here will enable future studies to collect larger datasets and compare motor unit organization across individuals, developmental stages, and species.

HDBSCAN was used for *E. berryi* during initial exploratory analyses, and Affinity Propagation was adopted for *S. officinalis* because it better captured the correlation structure of those recordings. We did not re-analyze the *E. berryi* data with Affinity Propagation, and the implications of algorithm choice are now discussed in the Discussion.

> ***Reviewer #2 (Public review):***
>
> *Summary:*
>
> *Overall, this is an excellent paper, making use of a newly developed system for monitoring the behaviour of chromatophores in the skin of (mostly) free-swimming bobtail squid and European cuttlefish. The manuscript is very well-written, clearly presented and very well-structured. The central finding, that individual chromatophores are connected to multiple motor neurones, is not new. Novelty instead comes from the ability to measure the actuation of chromatophore sections across wide areas of skin in free-swimming animals, showing the diversity of local motor units and reinforcing the notion that individual chromatophores are not necessarily the individual units of colour change, but rather local motor units that cover multiple neighbour and near-neighbour*

> *chromatophore muscles. This is an excellent finding and one that will shape our understanding of the neural control of cephalopod skin colour.*
>
> *Strengths:*
>
> *The methodological approach to collecting large amounts of data about local variations in the expansion of sections of chromatophores is exciting, and the analysis pipeline for clustering sections of chromatophores whose spontaneous activity correlated over time is powerful and exciting.*
>
> *Weaknesses:*
>
> *Some minor edits and typographical errors need correcting. I also had some concerns that the preparation for the electrophysiological section of the manuscript complies with the journal's ethical requirements, so I would urge that this be carefully checked.*

We thank the reviewer for the positive evaluation of our work and for recognizing the value of the methodological approach and the clarity of the manuscript.

We have carefully reviewed the manuscript and corrected minor typographical errors.

Regarding the ethical considerations raised for the electrophysiological experiments, we have carefully verified that the experimental procedures comply with the journal's ethical requirements and relevant institutional guidelines.

> ***Reviewer #3 (Public review):***
>
> *Summary:*
>
> *This study uses high-resolution videography and a custom computer-vision pipeline to dissect the motor control of cephalopod chromatophores in Euprymna berryi and Sepia officinalis. By quantifying anisotropic chromatophore deformations and applying dimensionality reduction methods, the authors infer that individual chromatophores can be a part of multiple motor units. Clustering analyses reveal putative motor units that often span multiple chromatophores, with diverse and overlapping geometries. Chromatophore expansion dynamics are faster and more stereotyped than relaxation, consistent with active neural contraction followed by passive recoil. Together, the results show that chromatophores function not as uniform pixels but as fractionated, coordinately controlled elements that enable flexible pattern generation*
>
> *Strengths:*
>
> *The authors present compelling, direct evidence that a). chromatophore deformations are anisotropic, and indirect evidence that b) individual chromatophores can be split across multiple putative motor units. This evidence is provided through data collected over large spatial scales, but also at a sub-chromatophore resolution. This combination of scale and resolution is not possible using traditional neuroanatomical and physiological approaches alone.*
>
> *The authors also develop a new non-invasive, image analysis approach to extract information about chromatophore deformation across large spatial scales on the organism's body. In principle, this approach is applicable across species and may allow for further comparative characterization of chromatophore motor control. It is therefore a promising new tool and useful resource for the community.*
>
> *Weaknesses:*
>
> *An important weakness of the work is that the methods the authors develop can only be applied during resting, spontaneous 'flickering' activity of chromatophores. The inability*

to reliably apply their technique during any kind of realistic camouflage is a large limitation, as it means this method cannot be used to study the dynamics of motor control during realistic camouflage behaviors.

Another weakness of this paper is the rather limited electrophysiological validation of the computational findings. The authors present only one electrophysiology experiment in E. berryi, the species that they used only for 'methodological development' and not for detailed characterization. A complementary electrophysiological experiment in S. officinalis, or some visualization of neuron morphology confirming that motor neurons do indeed project to multiple chromatophores, would strengthen the generalizability of their computational analysis. This would be particularly pertinent to validate the author's claim that some motor units contain chromatophores that are quite distant from one another on the animal.

Overall, the authors' technical contributions and method development are an important advance. This work serves as an excellent proof of concept that their method can extract useful information about chromatophore motor control. Further validation of their method is needed to fully trust the fine-scale conclusions drawn about the distribution and composition of multi-innervated chromatophores. Furthermore, the authors raise many interesting ideas about developmental constraints on circuit wiring and potential adaptive significance of multi-innervated chromatophores for certain features of camouflage patterning. Their method may be able to help resolve some of these questions in the future if it is refined and applied across developmental stages, regions of the animal, and across species

We thank the reviewer for their thoughtful evaluation and for recognizing the potential of the computational approach introduced in this study.

Regarding the focus on spontaneous chromatophore activity, we have clarified earlier in the Results section why these events are necessary to isolate individual muscle activations. While large camouflage patterns are visually striking, they involve the coordinated activation of many groups of chromatophores by premotor circuits simultaneously, making the identification of individual motor units, our goal here, impossible. Our approach can, however, also be applied during active behavior, including camouflage; the questions addressed there would be different, focusing on how multiple motor units are coordinated to generate the resulting skin patterns, rather than resolving the structure of single motor units. This could be challenging if the patterns of premotor control are highly variable, thus making the detection of meaningful or interpretable motion correlations difficult. This remains to be tested.

We also acknowledge that electrophysiological validation remains limited. Patch-clamp experiments were performed in *Euprymna berryi* to test predictions generated by the computational analysis, and these experiments confirmed that activation of single motor neurons can produce anisotropic expansion of chromatophore subregions. We now provide the associated datasets in the Data Availability section. We agree that complementary electrophysiological or anatomical experiments in *Sepia officinalis* would further strengthen the conclusions. Such experiments represent an important direction for future work.

> ***Recommendations for the authors:***
>
> ***Reviewer #1 (Recommendations for the authors):***
>
> *General points:*
>
> *(1) Given all the experimental conditions and animals tested, the manuscript would be much stronger if the figures represented pooled data from many animals and experiments (e.g. Figure 1C).*

We agree that pooling data from multiple animals would strengthen the manuscript. In practice, we tested these experimental conditions across several animals (14 *Euprymna berryi* and 12 *Sepia officinalis*), but we selected the segments shown in the figures for their minimal artifacts and errors. Acquiring high-quality, stable recordings of this type is extremely challenging, and the presented data represents the clearest examples suitable for analysis and visualization. We hope that in the future these methods will enable not only the collection of a larger, high-quality dataset, but also comparisons across individuals, ages, species, and different regions of the mantle.

> *(2) It's very unclear what animals were used for each experiment:*
>
> *(a) E. berryi: L677 states that 14 animals were filmed, and L684 implies that non-sedated individuals were used in addition to sedated animals, but it appears all the data is from a single E. berryi with sedation?*

The original wording was unclear, so we modified the sentence for clarity. The Methods now specify that 14 animals were filmed to refine the experimental pipeline and explore different conditions, while the data presented in the Results are from a single lightly sedated individual chosen for quality and stability of chromatophore activity.

> *(b) S. officinalis: L692 onwards states that lots of different conditions and animals were explored, but only minimal data from a couple of animals is described in the figures. L156 states that all (?) the data comes from one head-fixed animal and one sedated and head-fixed animal. L549: The conclusion states that the pipeline was used in freely moving animals, but it appears that all of the S. officinalis were head-fixed? This is very confusing. Rather than describing the conditions of every experiment ever performed, the manuscript would benefit from explicitly stating the experimental conditions used for each figure.*

The original text was unclear. We have clarified in the manuscript which animals and experimental conditions were used for the analyses in each figure. To clarify, *E. berryi* was recorded without head fixation, whereas *S. officinalis* data were obtained under head-fixed conditions. We did film 11 *S. officinalis* without head fixation, and data can in principle be extracted from these recordings. Head fixation was used both to minimize visual artifacts and to enable longer, stable recordings, which was important for capturing the highest level of apparent noise in motor unit activation—information that is critical for our analyses of motor-unit organization, though not necessary for studies of broader camouflage patterns. Our computational pipeline enables large-scale analyses that would be very difficult or impossible with traditional electrophysiology, not that all data were acquired from freely behaving animals. While fully unconstrained recordings remain technically challenging due to optical and logistical constraints, we maintain that our approach provides a valid framework for analyzing freely behaving animals.

> *(c) Additionally, there is a claim that the sedated condition represents the unsedated one (e.g. L151 and L643), but no data is shown to support this. L173 references Figure 6d as evidence, but 6d doesn't exist. Only L210 provides sedation/no sedation statistics for the*

> *number of components per motor unit. However, in L643 it says "and motor unit organization remained unchanged". This data needs to be shown to include that statement.*

Reference to the inexistant 6d figure was removed. L170 provides statistics for the number of principal components per chromatophore, and L210 provides statistics for the number of components per MU. We do not think a sub-figure is necessary. We, however, agree that L643 “motor unit organisation” is potentially misleading as we only compared the number of chromatophores belonging to a single MU and not the MU shape or distribution. Changed “organization” to “size (in chromatophores)”.

> *(3) The text needs considerable revision. There are many typos (including multiple instances of "refs" instead of the actual references being inserted). These issues make the manuscript much more difficult to evaluate.*

Our apologies. We have now added the missing refs.

> *(4) It is not clear how convincing the chromatophore groups are. For instance, Figure 4h could alternatively be interpreted as a group of 5 chromatophores in a motor group that happen to co-vary with a sixth one at a great distance. Without seeing some of the raw data (videos), it's difficult to assess how convincing it is that these chromatophores belong to the same group. I recommend analyzing: when multiple chromatophores expand together, what is the likelihood that other chromatophores also happen to expand at the same time (given the frequency that they're all changing shape spontaneously)?*

We appreciate the reviewer’s concern. Chromatophores are assigned to the same cluster because their activity, or that of their slices, covaries consistently over time. It is, of course, possible that what appears as a single motor unit may reflect two or more motor neurons acting simultaneously during the recording. Longer video segments increase confidence in the integrity of inferred motor units, but in the absence of a ground truth for motor unit spatial organization in this species at this age, it is difficult to quantify the likelihood that two motor units are being conflated. Raw video data is provided in the Data Availability section. We note, however, that most of the time motor units cannot be readily discerned by eye, because individual chromatophores and their constituent slices fluctuate continuously, and motor-unit correlations are subtle and distributed across multiple chromatophores.

> *(5) The rationale for focusing on spontaneous activity is introduced relatively late in the manuscript and would benefit from being stated earlier. Examples should be provided of what this looks like (as opposed to regular chromatophore expansion). It would be valuable to see measurements across many experiments of how expanded the chromatophores are - what is the change in surface area? And what is the frequency of expansion for each chromatophore?*

Thank you for the remark. This is true. We have added a paragraph at the beginning of the Results section to clarify the rationale for focusing on spontaneous activity.

This section now reads:

“Because our primary aim was to describe the composition and coordination of chromatophore motor units, it was important to examine animals in the absence of the descending commands that occur during active behavior. Spontaneous activity, typically mild and “noisy” was thus ideal to enable measurements of the motion correlations between chromatophores that reflected shared motor neuron drive, rather than shared correlations due to upstream motor neuron groupings by premotor circuits.”

We added an example of video recording of spontaneous activity in our Data Availability section.

While quantifying expansion magnitude and frequency across experiments would indeed be valuable, these questions fall outside the primary focus of the present study, which centers on resolving motor unit organization. In the section “Dynamics of chromatophore expansion and contraction,” we analyze the speed of expansion and contraction to demonstrate that such kinetic features can be reliably detected with the temporal resolution of our video imaging approach. By isolating single muscle activations, we establish a methodological framework that can be used in future work to quantify expansion amplitude, rate of change and frequency across preparations.

> *(6) Chromatophore expansion was only measured in anesthetized E. berryi, and L679 states that chromatophore expansion was triggered by shining light on the skin. However, light-mediated chromatophore expansion may be mediated by a different mechanism, so chromatophore correlations do not necessarily reflect the underlying motor control.*

We agree that there is, in principle, a theoretical risk of direct light-mediated activation of chromatophores. Yet, the kinetics of this light mediated activation are very different, and are the object of a separate, on-going investigation by our groups. In our experiments, the illumination was applied to the whole animal rather than locally to the skin, ensuring that all chromatophores and the eyes were exposed to the same light source. By transitioning from darkness to light, we created a window in which chromatophores were partially expanded—both fully contracted and fully expanded states would show little to no decorrelation. Within this window, we observed spontaneous fluctuations in chromatophore activity, which formed the basis for our correlation analyses. To our knowledge, direct light-mediated expansion of chromatophores has not been reported in *E. berryi* although it may exist there. Finally, the size, shape, and orientation of the inferred motor units align with electrophysiological evidence, supporting the validity of our motor unit inferences.

> *(7) Some figures might be better suited for the supplement. For instance, it's not clear what the significance of Figure 5 is (it's not currently sufficiently justified in the text).*

We have clarified the purpose of Fig. 5 in both the Results and Discussion sections. In the Results, we now explain that events are separated by amplitude to show that expansion–contraction kinetics can be reliably measured across a full range of chromatophore events, validating the precision of our videographic approach. In the Discussion, we highlight that this precision allows measurement of radial muscle speeds and opens avenues to study chromatophore biomechanics, including the contributions of intertwined forces such as radial muscles, elastic pigment sacs, and intercellular coupling.

> *(8) Multiple chromatophores can belong to multiple clusters - this study reveals that this is because subsections of a chromatophore are controlled separately. But do the same sections (slices) of chromatophores ever belong to multiple clusters?*

Yes, it is possible. Dubas (1985) used videographic recordings to show that the same chromatophore muscle fibers could be activated by stimulation of different nerve bundles, supporting Florey’s (1969) electrophysiological evidence for polyneuronal excitatory innervation. From Dubas: "Usually, different muscle fibres were recruited by each nerve but sometimes a single muscle fibre responded to stimulation of each nerve. Variations of the stimulus voltage also produced gradation of the amplitude of shortening of individual muscle fibres. This supports the evidence above for multiple innervation of single muscle fibres."

The petal-like distribution of motor-neuron influence shows overlapping territories, suggesting that some chromatophore sections may be influenced by multiple neurons.

However, this overlap could arise from polyinnervation of individual muscles, the presence of gap junctions between muscles, or passive mechanical coupling due to the elastic properties of the pigment sac.

The petal-like distribution of motor-neuron influence shows overlapping territories, suggesting that some chromatophore sections may be influenced by multiple neurons. However, this overlap could arise from polyinnervation of individual muscles, the presence of gap junctions between muscles, or passive mechanical coupling due to the elastic properties of the pigment sac.

With the present approach, it is not possible to disentangle the relative contributions of these mechanisms, which will require targeted physiological or anatomical experiments. For this reason, we adopted a hard clustering approach for individual chromatophore slices.

> *(9) All time should be labeled in seconds, not in frames, and all distances should be measured in um or mm, not in pixels.*

We chose to present figures in pixels and frames to reflect the native units of our recordings and analyses, which preserves fidelity and reproducibility of the computational pipeline. For biological interpretation, corresponding values are converted to μm in the main text, providing the relevant real-world scale. A scale for conversion is provided in the figure legend.

> *Specific comments:*
>
> *(1) L36: I'm not sure the description of virtual chromatophores here is clear enough to make sense to a more general audience.*

Addressed. We retained the concept of ‘virtual chromatophores’ in the abstract and added a brief clarifying phrase to indicate that these are functional groupings of adjacent chromatophore territories that act as single units.

> *(2) L50: "Rimmed by" - consider rephrasing.*

Addressed. Replaced with “surrounded”.

> *(3) L64: "refs" - actual references aren't inserted. There are multiple other examples of this.*

Addressed. Added missing references.

> *(4) L100: This section could use rewriting. Some of the text reads more like a figure legend.*

Addressed. We have streamlined the main text to reduce redundancy with the figure legend.

(5) L101: Consider the opening sentence/s providing a more general introduction to the question and approach.

Addressed.

> *(6) L104: This implies that the data presented are from 14 animals of many ages. This is only relevant if the pooled data is analyzed and presented.*

We agree that the original phrasing was ambiguous. We have modified the sentence for clarity, and explain in the Methods that 14 animals were filmed to refine the pipeline and explore experimental conditions, while the analyses shown are from a single animal.

> *(7) L111: HDBSCAN should be defined.*

Addressed. The acronym has been expanded.

> *(8) L173: Figure 6D doesn't exist.*

Addressed. Reference to the inexistent 6d figure was removed.

> *(9) L193: "excluding negative (contraction) phases" This phrase requires clarification.*

Addressed. Added “see Methods” in the legend and added clarification on the reasoning in Methods.

> *(10) L204: Should explain why the switch to affinity-propagation clustering was made when a different method was used for E. berryi.*

Addressed in discussion.

> *(11) Figure 3: I recommend including a diagram or image of a whole cuttlefish and showing what the corresponding imaging area was in relation to the animal so the reader gets an intuitive sense of scale.*

Thank you. We have added a supplementary figure to give the reader a sense of scale.

> *(12) L221/Fig 3b: These colors are supposed to represent clusters of 3 to 5 chromatophores? The clusters look much bigger.*

The figure shows clusters of 3 to 5 chromatophores, but many adjacent clusters were assigned the same color. We have changed the colors to remove this ambiguity.

> *(13) Figure 3c: This would be more powerful if it represented the combined data of many experiments to draw a general conclusion. Also, shouldn't these cluster sizes match those in 2e, e.g. they get as big as 40?*

We assume the reviewer is referring to a comparison between Figures 3c and 2e. For visualization purposes, the graph in 3c was truncated to display over 90% of the data, which explains why the largest clusters appear smaller than in 2e. We modified the legend accordingly. We agree that the results would be strengthened by pooling data from additional experiments; however, acquiring high-quality, artifact-free recordings suitable for motor unit analysis is extremely challenging. We hope that our framework will enable future studies to extend this analysis.

> *(14) Figure 4: I would show some of these examples earlier, to give the reader an intuitive sense of the data and claims (though it doesn't need its own figure - provide a couple of examples, and the diagram of how much of the mantle you're sampling) then put the rest in the supplement, and include some videos too.*

We agree that providing spatial context is important for readers to develop an intuitive understanding of the dataset. However, introducing examples of motor units earlier in the manuscript would, in our view, interrupt the logical progression of the Results, where motor unit identification builds on prior analyses. To address the reviewer’s concern, we have added a new supplementary figure (Fig. S1) illustrating the size and location of the sampled mantle region. In addition, we now provide representative videos in the Data Availability section to give readers direct visual access to the underlying dynamics.

> *(15) Figure 4f: Is the location of the split color in each dot accurate? It's surprising that each one is split down the middle, and the pink side is always on the right - this is unintuitive given where the motor neuron is likely to be located.*

The dots and half dots represent the membership of a chromatophore to a particular cluster.

> *(16) Figure 5: I didn't find this figure sufficiently justified in the text. I would move this to the supplement.*

Addressed in General point #7.

> *(17) L350: States that 12 animals were patched, but the data isn't shown. It's important to show all of this data (some of which can be in the supplement).*

Addressed. We provided the data in the Data Availability Section.

> *(18) Figure 5: I would quantify how many chromatophores were in each motor group across all the recording sessions, and compare this to the equivalent behavioral analysis.*

We assume the reviewer means Fig. 6. We calculated and stated the size of motor units across patching sessions.

> *(19) Figure 5c: I recommend labeling each panel with a different number so you can refer to specific data.*

We assume the reviewer means Fig. 6c. We consider the figure layout clear enough to allow readers to follow the data without additional panel numbers.

> *(20) L379: Typo: repeat of "quantitative"*

Addressed.

> *(21) L576: Salinity should be 33-36 ppt, not %*

Addressed.

> *(22) L877: The salinity units are sg? That should be stated. Though I would use the same units for salinity throughout.*

Addressed.

> *Overall, this work introduces a potentially valuable quantitative framework for studying chromatophore dynamics. Addressing the points above would substantially strengthen the manuscript and clarify the scope and support for its conclusions.*

We thank the reviewer for these many helpful comments.

> ***Reviewer #2 (Recommendations for the authors):***
>
> *(1) Line 64 - missing references for chromatophore colour with age.*

Addressed. Added missing refs.

> *(2) Line 64-65 - would be good to have a little more detail about what is meant by 'migrating through the skin'. Is this a lateral process, or depth in the skin?*

Addressed. Changed “migrating in the thickness..” with “through the thickness..” to emphasize verticality.

> *(3) Line 72 - typo, should read '...individual and groups...'*

Addressed.

> *(4) Remove 'In Fig 1, ...' from line 104.*

Addressed.

> *(5) Figure 1 - It's unclear why some chromatophores are uncoloured with a red dot in the centre. Are these chromatophores that do not share a cluster with neighbours? If so, wouldn't it make more sense to colour the chromatophore with a unique colour of its own? Or, at the very least, make a note in the caption to indicate that all white chromatophores are not clustered with neighbours.*

Segmented chromatophores are shown in white, with coloured slices highlighting cluster membership. Uncoloured slices represent outliers. Addressed in the figure legend.

> *(6) Line 119 - the concept of a 'closed virtual chromatophore' needs a few more words of explanation. The way I interpret the text as it is, is that the motor units driving colour change are not necessarily the individual chromatophores, but a motor region containing a mixture of whole and partial chromatophores innervated by the same motor neuron. If this is the case, a few extra words of description would help here to remove any ambiguity as I think this is an important concept for the paper.*

Addressed. We added a sentence clarifying the concept.

> *(7) Line 173 - Figure 6d doesn't exist in the paper. Was a different panel intended? If so, please make sure to number the figures in order of appearance in the manuscript.*

Reference to the inexistent figure 6d was removed.

> *(8) Figure 3b is very difficult to see. Perhaps consider lightening the background image. Please also indicate whether the individual colours refer to individual clusters. If this is the case, then some of these clusters look much larger than the 3-5 suggested in the caption.*

This issue has been corrected.

> *(9) Line 210 - remove the bold type.*

Addressed.

> *(10) Line 211 - please specify which 'two groups' you are referring to here. Presumably, this is anaesthetised and non-anaesthetised.*

Addressed.

> *(11) I think that the text is missing any indication of the pixel sizes involved in extracting slice metrics, particularly from the S. officinalis data. It would be great to include some data on how many pixels span the radius of an expanded chromatophore. There is some small indication of this in Figure 2a, but a panel or two with details about the pixel size of S. officinalis chromatophores and their slices would be welcome. This would help with the judgment of the robustness of the resolution of the analysis. Looking at the y-axis in Figure 5a, there is some indication that the chromatophore radius is only 1 to 8 pixels. Is this the case?*

Figure 5a doesn’t show chromatophore radius but instead the relative change in peak amplitude during an expansion event. At that point the chromatophore has likely a larger radius as you sum the baseline radius of the chromatophore + the size of the peak.

> *(12) Line 246-7 - reword this sentence to avoid referring to Figure 3d in the narrative. Include it in parentheses instead.*

Addressed.

> *(13) Lines 408 and 409 - missing references.*

Addressed.

> *(14) Line 576 - salinity should be reported in parts per thousand, not per cent.*

Addressed.

> *(15) Line 593 - how were animals <50mm fed?*

Animals smaller than 50 mm were fed Neomysis spp. or small Palaemonetes spp., as noted a few lines above the description for animals larger than 50 mm.

> *(16) Line 847 - typo - '...putative motor units' ramifications...'*

Addressed.

> *(17) Line 854 - better to write out the [chrom_id, label] info as narrative text rather than using the variable names.*

Addressed.

> *(18) Line 876 - two typos '...were reared in an artificial...'*

Addressed.

> *(19) Line 877 - please use the same salinity metric as used in the earlier part of the methods.*

Addressed.

> *(20) Section 898-910 - equipment details would ideally include the location of the company. E.g. (BX51W1, Olympus, Tokyo, Japan).*

Addressed.

> ***Reviewer #3 (Recommendations for the authors):***
>
> *I am left with a number of questions that arise from the authors' work, some of which the authors themselves briefly mention in the technical limitations section.*
>
> *(1) In relation to the first weakness, do the authors know if the recruitment patterns they identify are likely to be the same when octopi perform visually-mediated camouflage to their environment?*

Thank you for this comment. We assume the reviewer is referring to *S. officinalis*. There seems to be a misunderstanding: our approach is designed to reveal the smallest independent functional units—motor units—that together generate skin patterns. The technique is fully applicable to an animal displaying camouflage, but the results would necessarily differ. Camouflage patterns are composed of relatively large shapes compared to individual motor units and arise from the coordinated activation of multiple units. Disentangling motor units requires decorrelated activity, whereas visually-evoked camouflage inherently drives correlated motor-unit activation by premotor control. To use an analogy, if our goal were to map the distribution and wiring of pixels on a screen, it would be more informative to broadcast a noise signal rather than display coherent images, as the noise produces decorrelated activity that allows the underlying structure to be resolved. We have clarified this important point in the early results section.

> *(2) The authors provide indirect evidence that motor neurons innervate multiple chromatophores. Can sets of radial muscles within a chromatophore be innervated by*

> *multiple motor neurons? Is there neuroanatomical evidence or experiments that could perhaps shed light on this?*

Addressed above. Same question as #1(8).

> *(3) Are multi-innervated chromatophores evenly distributed across the octopus's body? For instance, could the authors compare chromatophore recruitment over multiple patches on the animal from multiple regions?*

At present, we do not have sufficient data to quantitatively compare motor-unit structure or the distribution of multi-innervated chromatophores across different body regions of cuttlefish. However, we would not necessarily expect uniformity across the skin, as distinct body regions are associated with characteristic pattern elements (e.g., the white square on the central mantle or the thicker zebra stripes along the sides). It is therefore plausible that different motor-unit geometries and densities are differentially represented across regions to support these region-specific patterns. Future recordings spanning multiple patches and body locations will be required to test this question directly.

> *(4) Relatedly, is there any idea of whether chromatophore size or age corresponds with the number of motor units within a single chromatophore?*

At present, our analyses are limited to single developmental time points, and we therefore cannot directly assess whether chromatophore size or age correlates with the number of motor neurons innervating an individual chromatophore. However, this is a question that our analysis framework is explicitly designed to address. Our custom pipeline, CHROMAS, (Ukrow, Renard et al., 2025) includes tools for longitudinal image alignment that allow chromatophores to be tracked within the same animal across development. Applying these scripts to developmental datasets enables future analyses linking chromatophore growth or age to changes in the motor innervation of single chromatophores.

> *I understand that a full resolution to the issues raised above may require substantial additional experiments. At a minimum, further discussion of these points with integration of existing literature would elevate the paper.*

https://doi.org/10.7554/eLife.110074.2.sa0